Endostructural morphology in hominoid mandibular third premolars: Geometric morphometric analysis of dentine crown shape

Thomas W. Davies[a,b,*], Lucas K. Delezene[c], Philipp Gunz[b], Jean-Jacques Hublin[b], Matthew M. Skinner[a,b]

[a] *School of Anthropology and Conservation, University of Kent, Canterbury, CT2 7NZ, UK*

[b] *Department of Human Evolution, Max Planck Institute for Evolutionary Anthropology, Deutscher Platz 6, 04103 Leipzig, Germany*

[c] *Department of Anthropology, University of Arkansas, Fayetteville, Arkansas, 72701 USA*

*Corresponding author.

E-mail address: thomas_davies@eva.mpg.de (T.W. Davies)

Keywords: Premolars; Enamel-dentine junction; Molarization, Geometric morphometrics; Taxonomy; Dental morphology

Acknowledgements

For access to specimens, we would like to thank Bernhard Zipfel, Lee Berger, Sifelani Jira (Evolutionary Studies Intitute, University of the Witwatersrand), Miriam Tawane (Ditsong Museum), Job Kibii (National Museums of Kenya), Metasebia Endalemaw, Yared Assefa (Ethiopian Authority for Research and Conservation of Cultural heritage), Yoel Rak, Alon Barash, Israel Hershkovitz (Sackler School of Medicine), Michel Toussaint (ASBL Archéologie Andennaise), Jean-Jacques Cleyet-Merle (Musée National de Préhistoire des Eyzies-de-Tayac), Ullrich Glasmacher (Institut für Geowissenschaften, Universität Heidelberg), Frieder Mayer and Christiane Funk (Museum für Naturkunde - Leibniz Institute for Evolution and Biodiversity Science), Jakov Radovčić (Croatian Natural History Museum), Christophe Boesch and Uta Schwarz (Max Planck Institute for Evolutionary Anthropology) and the Leipzig University Anatomical Collection (ULAC). For project support we thank Zeresenay Alemseged and Bill Kimbel. We would also like to the reviewers, the associate editor and the editor for their helpful comments and guidance, as well as Ottmar Kullmer for comments on an earlier version of this manuscript. This work was funded by the Max Planck Society, and financial support for L.K.D. was provided by a Connor Family Faculty Fellowship and the Office of Research and Development at the University of Arkansas.

Endostructural morphology in hominoid mandibular third premolars: Geometric morphometric analysis of dentine crown shape

Abstract

In apes, the mandibular third premolar (P_3) is adapted for a role in honing the large upper canine. The role of honing was lost early in hominin evolution, releasing the tooth from this functional constraint and allowing it to respond to subsequent changes in masticatory demands. This led to substantial morphological changes, and as such the P_3 has featured prominently in systematic analyses of the hominin clade. The application of microtomography has also demonstrated that examination of the enamel-dentine junction (EDJ) increases the taxonomic value of variations in crown morphology. Here we use geometric morphometric techniques to analyze the shape of the P_3 EDJ in a broad sample of fossil hominins, modern humans, and extant apes (n = 111). We test the utility of P_3 EDJ shape for distinguishing among hominoids, address the affinities of a number of hominin specimens of uncertain taxonomic attribution, and characterize the changes in P_3 EDJ morphology across our sample, with particular reference to features relating to canine honing and premolar 'molarization'. We find that the morphology of the P_3 EDJ is useful in taxonomic identification of individual specimens, with a classification accuracy of up to 88%. The P_3 EDJ of canine-honing apes displays a tall protoconid, little metaconid development, and an asymmetrical crown shape. Plio-Pleistocene hominin taxa display derived masticatory adaptations at the EDJ, such as the molarized premolars of *Australopithecus africanus* and *Paranthropus*, which have well-developed marginal ridges, an enlarged talonid, and a large metaconid. Modern humans and Neanderthals display a tall dentine body and reduced metaconid development, a morphology shared with premolars from Mauer and the Cave of

Hearths. *Homo naledi* displays a P_3 EDJ morphology that is unique among our sample; it is quite unlike Middle Pleistocene and recent *Homo* samples and most closely resembles *Australopithecus, Paranthropus* and early *Homo* specimens.

1. Introduction

The mandibular third premolar is morphologically variable among hominoids, due in large part to a difference in function of the tooth between hominins and apes (non-hominin hominoids). In apes, as in other catarrhines, the P_3 forms part of the canine honing complex. This is reflected in the morphology of the tooth: a high protoconid creates a tall crown, while the crown base is asymmetric, creating a long and broad buccal sloping surface along which the upper canine is honed. Canine honing is absent in *Australopithecus* (Robinson, 1956; Le Gros Clark, 1967; Johanson et al., 1978) and there is evidence for a lack of functional honing in earlier putative hominins (Brunet et al., 2002; Suwa et al., 2009). However, many of the P_3 features associated with canine honing were retained for some time. For example, the P_3 in *Ardipithecus ramidus* is described as having a tall total crown height and very little metaconid development (White et al., 1994; Suwa et al., 2009), and similarly, *Australopithecus anamensis* displays a high and sharp P_3 protoconid, and only minimal development of the metaconid (Ward et al., 2001).

P_3 features relating to canine honing were eventually lost, however, and we see substantial changes in P_3 morphology in *Australopithecus* and *Paranthropus*, related to a changing functional role of the tooth during mastication. Specifically, a number of species display 'molarized' premolars that possess a suite of features resulting in an expansion of the talonid and the addition of extra cusps and/or cuspules (Wood and Uytterschaut, 1987). These adaptations may serve to increase the masticatory capabilities of the P_3 (Leonard and Hegmon, 1987), and are most extreme in *Paranthropus*, where they are accompanied by a

suite of dental characters that have been linked to forceful mastication using the postcanine dentition. These features include thick enamel (Conroy, 1991; Grine and Martin, 1988; Olejniczak et al., 2008), large postcanine teeth (Robinson, 1956; Tobias, 1967), small anterior teeth (Robinson, 1956; Tobias, 1967; Ungar and Grine, 1991), and robust mandibles (Robinson, 1956; Tobias, 1967; Wood and Aiello, 1998). The P_3 of Middle-Late Pleistocene hominins (*Homo heidelbergensis, Homo neanderthalensis,* and *Homo sapiens*) are also distinctive, showing a more symmetrical occlusal outline and a reduced talonid (Gómez-Robles et al., 2008). There is also a large amount of variation in P_3 morphology within modern humans related to differences in crown shape, cusp number and root form (Kraus and Furr, 1953; Sakai, 1967; Scott and Turner, 1997; Cleghorn et al., 2007).

These trends make the P_3 of particular interest to those studying human evolution. However, as with any study of tooth morphology, a significant problem for analyses is the erosion of dental characteristics through tooth wear. In response, researchers have increasingly used microtomography to image the enamel-dentine junction (EDJ), which is often preserved in specimens with moderate tooth wear, allowing for the inclusion of specimens that would otherwise be undiagnostic. The EDJ and the outer enamel surface (OES) have a high level of correspondence (Nager, 1960; Skinner et al., 2010; Ortiz et al., 2012; Morita et al., 2014; Guy et al., 2015) since the majority of the distinctive features of the OES originate at the EDJ.

The EDJ has been particularly useful in geometric morphometric (GM) studies, as the sharper appearance of dental features allows for reliable placement of landmarks and semilandmarks (Skinner et al., 2008). GM provides a powerful method of biological shape analysis, and can be useful for quantifying morphological changes in dental studies (Gómez-Robles et al., 2008; Singleton et al., 2011; Carayon et al., 2019), as well as in addressing issues of hominin taxonomy (Skinner et al., 2008; Zanolli and Mazurier, 2013; Martin et al.,

2017; Hublin et al., 2017; Hershkovitz et al., 2018). Typically these studies focus on mandibular and maxillary molars, although a number of studies have performed GM analysis of the EDJ of multiple tooth positions, including mandibular premolars (Braga et al. 2010; Pan et al., 2017; Zanolli et al. 2018).

Here, we will use GM techniques to analyse the P_3 EDJ morphology of a selection of extant apes, modern humans, and fossil hominins, with three main aims:

(1) To characterize the P_3 morphology of a variety of hominoid taxa, and explore the EDJ manifestation of traits relating to canine honing and molarization
(2) To evaluate the taxonomic potential of the P_3 EDJ shape to discriminate among hominoid taxa
(3) To assess the taxonomic affinity of indeterminate specimens.

A second companion paper will characterize the EDJ expression of a number of discrete P_3 traits (Davies et al., under review).

2. Materials and methods

2.1. Study sample

The study sample was chosen to represent as many taxa within the hominin clade as possible, as well as extant apes and modern humans. However, the sample is limited by the availability of CT scans, and the ability to extract the EDJ surface from those scans. Therefore, some taxa are unrepresented, or represented by relatively few specimens.

The sample is summarized in Table 1 (a full list of specimens can be found in Supplementary Online Material [SOM] Table S1), and consists of 111 P_3, of which 99 are assigned to species rank. Seven specimens are grouped as *Homo* sp. (including those assigned

to *Homo habilis*, *Homo rudolfensis*, and *Homo ergaster*), and five are considered indeterminate.

Specimens from Qafzeh are included here, but will be separated from the recent *H. sapiens* sample, which is derived from an anatomical collection of recent modern humans. The recent *H. sapiens* sample is curated at the University of Leipzig Anatomical Collection (ULAC). Relatively little information is available on the provenance of this sample, but the available information is presented in SOM Table S3.

2.2 Terminology

Terminology used to describe P3 morphological traits can vary between authors. The terms used here are explained in Figure 1. Of particular importance is the discussion of crown height; total crown height refers to the distance between the cervix and the tip of the tallest cusp (typically the protoconid). However, at the EDJ it is clear that this can be divided into two components; dentine body height and dentine horn height. Here, dentine body height refers to the distance between the cervix and the occlusal basin, while dentine horn height refers to the distance between the occlusal basin and the tip of the tallest dentine horn. It should be noted that in the GM analysis used here, the occlusal basin is not directly measured, so instead the height of the marginal ridges is used. Although there is some variation in the height of the marginal ridges above the occlusal basin at the EDJ, our observations suggest this is minimal.

2.3 Microtomography

Microtomographic scans of the premolar sample were obtained using either a SkyScan 1173 at 100–130 kV and 90-130 µA, a BIR ACTIS 225/300 scanner at 130 kV and 100–120

μA, or a Diondo d3 at 100–140kV and 100–140 μA, at the Department of Human Evolution, Max Planck Institute for Evolutionary Anthropology (Leipzig, Germany). They were then reconstructed as 8-bit TIFF stacks (isometric voxel resolutions ranging from 13–45 μm).

2.4 Image filtering

The image stacks for each premolar were filtered using a 3D median filter, followed by a mean of least variance filter, both with a kernel size of either one or three, implemented using MIA open source software (Wollny et al., 2013). This process facilitates the segmentation of enamel from dentine by improving the homogeneity of the grayscale values for the enamel and dentine, and by sharpening the boundaries at the interface between tissue types (Schulze and Pearce, 1994). The kernel size was decided by manually assessing the level of contrast between enamel and dentine; a kernel size of three was used on those scans with low contrast. The effect of filtering on the morphology of the EDJ has previously been shown to be minimal (Skinner, 2008).

2.5 Tissue segmentation

The filtered image stacks were processed using Avizo 6.3 (Visualization Sciences Group, 2010) in order to produce surface models of the EDJ. Enamel and dentine were segmented semiautomatically using grayscale values in the 3D voxel value histogram. In some cases, less distinct tissue classes made segmentation through this method not possible, and instead a seed growing algorithm was employed to segment enamel from dentine, before being checked manually. A triangle-based surface model of the EDJ was produced in PLY format, using the unconstrained smoothing parameter in Avizo.

In some specimens, dental wear had removed the tips of dentine horns. In the case of specimens with minimal wear, the missing portion of the dentine horn was reconstructed following the procedure of Skinner (2008). This procedure is similar to correcting for interstitial wear, and involves inferring the structure of the dentine horn tip from the preserved anatomy of the dentine horn. This procedure was restricted to specimens for which less than a quarter of the dentine horn was missing—estimated through viewing the EDJ in side view. Specimens considered for reconstruction were restricted to those showing wear less than wear level 3 according to Molnar (1971). This procedure was also restricted to cases in which multiple observers were confident of the original position of the dentine horn using their experience, anatomical knowledge, and the preserved EDJ morphology. The dentine horns were reconstructed using Geomagic Studio 2014 (3D systems, Rock Hill) and reconstructed specimens are marked in SOM Table S1. The EDJ of specimens with substantial cracks were realigned using Geomagic Studio.

2.6 Landmark collection

3D landmarks were collected in Avizo 6.3 in three distinct sets; ‘EDJ main’, ‘EDJ ridge’ and ‘CEJ ridge’ (CEJ = cementum-enamel junction). EDJ main and EDJ ridge landmarks were placed directly on the EDJ surface model. EDJ main consists of two landmarks, the first placed on the tip of the protoconid, and the second placed on the metaconid, where present. For specimens where a metaconid was not present, the landmark was placed on the equivalent position, where the transverse crest meets the lingual segment of the mesial marginal ridge (Fig. 1). In apes, the transverse crest often does not reach the marginal ridge, so for these specimens, the second EDJ main landmark was placed on the lingual margin of the crown, mesiodistally level with the transverse crest. EDJ ridge landmarks were placed around the marginal and protoconid crests encircling the basin of the tooth, beginning at the

protoconid landmark, and running mesially, eventually returning to the protoconid (Fig. 1). In some specimens, the mesial or distal marginal ridge is partly flattened; in these cases we placed landmarks along the equivalent points along the flattened EDJ surface. CEJ ridge landmarks were placed on an isosurface rendering of the external surface of the tooth. When the CEJ is obscured on the isosurface rending by matrix build-up or the presence of an adjacent tooth, the unfiltered image stack was instead used to locate the CEJ and place landmarks. The first landmark was placed on the CEJ at the midpoint of the buccal face of the tooth, then landmarks were placed mesially around the CEJ. In cases where part of the CEJ was missing, the location of these landmarks was estimated if it was considered that the original location of the CEJ could be reasonably estimated.

2.7 Derivation of homologous landmark sets

Geometrically homologous semilandmarks (Bookstein, 1997; Gunz et al., 2005) were derived using a software routine written by P.G. (Gunz et al., 2005; Gunz and Mitteroecker, 2013) implemented in Mathematica 10.4.1 (Wolfram Research, Inc., 2016). A smooth curve was fit through the landmarks of the EDJ ridge and CEJ ridge landmark sets using a cubic-spline function. For the EDJ ridge set, the EDJ main landmarks were projected on to the curve, dividing the curve into mesial and distal portions. A fixed number of initially equally spaced semilandmarks were placed along the curve; the EDJ had 20 landmarks in the mesial portion and 25 in the distal, whilst the CEJ had 40 landmarks. The number of semilandmarks for each curve was chosen in order to ensure that the shape variation present in each area is fully captured; a high level of sampling is important for creating visualizations in geometric morphometric analyses (Gunz and Mitteroecker, 2013). More landmarks are placed in the distal section of the EDJ ridge than the mesial section because this section is usually longer in hominins. EDJ main landmarks were fixed while those in EDJ ridge and CEJ ridge were

treated as semilandmarks, and allowed to slide along their curves so as to reduce the bending energy of the thin-plate spline interpolation function calculated between each specimen and the Procrustes average for the sample (Gunz et al., 2005; Gunz and Mitteroecker, 2013). The sliding operation was performed twice, after which the landmarks were considered to be geometrically homologous, and were then converted into shape coordinates using generalized least squares Procrustes superimposition, which removes scale, location, and orientation information from the coordinates (Gower, 1975; Rohlf and Slice, 1990; Goodall, 1991; Dryden and Mardia, 1998).

2.8 Analysis of EDJ and CEJ shape and size

For some specimens, it was not possible to place all landmarks, either due to dental wear beyond the level that could be reconstructed (as described above), poor contrast between enamel and dentine in the CT scan prohibiting the placement of EDJ landmarks (SOM Fig. S1), or, in some cases, due to incomplete crown development, meaning the CEJ has yet to form. In these instances, analyses were completed on subsets of landmarks, depending on the areas of morphology preserved. Ultimately, analyses were conducted in four groups, each utilizing different combinations of landmarks, to allow analysis of as many specimens as possible, and to assess the utility of these landmark sets for taxonomic distinctions. These are referred to as ‘EDJ+CEJ’, ’CEJ+Med’, ‘CEJ only’, and ‘EDJ only’. The EDJ+CEJ analysis uses all landmarks (as outlined in Fig. 1A). The CEJ only analysis uses only the landmarks from the CEJ ridge set, while the EDJ only analysis uses only landmarks from the EDJ main and EDJ ridge sets. The CEJ+Med analysis uses all landmarks from the CEJ ridge set, as well as a single fixed landmark placed on the metaconid (or equivalent point; marked as landmark 2 in Fig. 1A) as this was generally less worn than the protoconid.

The specimens included in each analysis are listed in SOM Table S1. A principal components analysis (PCA) was carried out using the Procrustes coordinates of each specimen in both shape and form space, the latter of which includes, as an additional variable, the natural logarithm of the centroid size of the specimen. This was completed for all four analyses. A permutation test was performed to test for shape differences between pairwise combinations of taxon groups. This was completed using Procrustes coordinates from the EDJ+CEJ analysis (as this analysis contains the maximum amount of shape information), and was limited to taxon groups containing three or more specimens (which excluded *P. boisei, Homo* sp*., H. ergaster,* and *H. heidelbergensis*). A separate permutation test was used to test for differences in centroid size between pairwise combinations of taxon groups. Here, the natural logarithm of centroid size for each specimen from the EDJ+CEJ analysis was used, and was again limited to taxon groups with three or more specimens. In both cases, the Benjamini-Hochberg procedure was used to control false discovery rate (Benjamini and Hochberg, 1995). Permutation tests were carried out in Mathematica 8.0, using 100,000 permutations.

For the purpose of assessing the classification accuracy of our analyses, canonical variates analysis (CVA) was used. A CVA creates a linear combination of variables such that the variation among predetermined groups is maximized, relative to the variation within the groups. In this case, the groups are the taxa to which the specimens have been assigned. This analysis was conducted separately for the EDJ+CEJ, CEJ+Med, CEJ only, and EDJ only analyses, and in each case, specimens were only included if they had been reliably assigned to taxa containing three or more specimens in all analyses (which excluded *P. boisei*, *Homo sp., H. ergaster,* and *H. heidelbergensis*). The specimens were classified using leave-one-out cross validation whereby each specimen is assumed to be unknown before being assigned to a group using the remaining dataset. A CVA requires that the number of variables be less than

the number of specimens, which is not possible in this case when using the Procrustes coordinates as variables, so instead we reduced the number of variables using the PCA and performed the CVA on limited numbers of principal components (PCs). For each analysis, the number of PCs was chosen such that they cumulatively explained 95% of the variance within the sample. The classification accuracy was then calculated as the percentage of specimens correctly classified using this method. The PCA and CVA, as well as the classification accuracy analysis, were conducted in R (R core Team, 2018).

2.9 Visualization of EDJ shape variation

3D PCA plots of the first three PCs were generated to visualize the variation in P_3 EDJ shape across the study sample. For this, specimens were split into three groups in order to allow clearer visualization of the shape differences present. Apes (*Hylobates*, *Pongo*, *Gorilla*, *Pan*) are grouped together, whilst hominins are split into two groups: Plio-Pleistocene hominins (*Australopithecus*, *Paranthropus*, early *Homo,* and *Homo naledi*), and Middle-Late Pleistocene hominins (*H. heidelbergensis, H. neanderthalensis*, and *H. sapiens*). 'Indeterminate' specimens are plotted in either the Plio-Pleistocene or Middle-Late Pleistocene groups, according to their proposed taxonomic affinities. Although *H. naledi* is Middle-Pleistocene in age (Dirks et al., 2017), it is included in the former group due to the morphology of the P_3, which is primitive for *Homo* (Berger et al., 2015; Irish et al., 2018), allowing clearer comparisons with the taxa it most closely resembles. A PCA plot with all taxa in the sample was also created in order to visualise larger-scale shape differences among taxa.

266 Wireframe models were used in order to visualize the mean landmark configuration for
267 each well-represented taxonomic group included in the full analysis. 3D PCA plots and
268 wireframe models were generated in Mathematica 8.0.

269

270 *2.10 Classification of additional specimens*

271 A number of specimens of uncertain taxonomic affinity were included, and will be
272 assessed with reference to the taxa present in our sample. Early *Homo* specimens SK 18a and
273 SKX 21204 have not been given a specific designation within *Homo*, but given that our
274 sample does not include *Homo habilis*, and the sample of other early *Homo* specimens here is
275 quite limited, we are not able to assess their species-level designation within *Homo*.

276

277 **3. Results**

278 *3.1. Changes in P_3 morphology through time*

279 Extant apes The P_3 in extant apes has a tall protoconid, a low dentine body height, and a CEJ
280 that is expanded mesiobuccally compared with hominins. The mesiobuccal expansion of the
281 CEJ also extends apically, giving the CEJ a sinusoidal shape, which, when viewed from the
282 lingual direction as in the wireframe models (Fig. 2), appears as a figure-of-eight.

283 The PCAs show clear separation among extant ape taxa in all three analyses (Figs. 3 and
284 4; SOM Fig. S2), although this separation is more marked in the analyses that include the
285 EDJ ridge, compared with the CEJ only analysis. Only differences between *Pongo* and the
286 other apes are significant in the shape permutation test (Table 3), although all pairwise
287 comparisons between these groups are significant in the size permutation test (Table 2).
288 *Pongo* is distinct in shape from the other apes due to a peak on the lingual side of the EDJ
289 ridge. This peak is caused by the extension of the transverse crest to the lingual margin of the

tooth where it meets the marginal ridge. Although this morphology is not seen in other extant apes in our sample, it is common in hominins. Other extant apes, particularly *Gorilla*, display a marginal ridge that is much lower (and therefore closer to the CEJ), resulting in a lower dentine body height. This feature is the main driver of the first principal component (PC1) for apes in Figures 3 and 4. As expected, the mean *Hylobates* P_3 centroid size is by far the smallest in the sample, whilst *Gorilla* is the largest (Fig. 5). The *Hylobates* P_3 is relatively mesiodistally longer, and buccolingually narrower, than the other ape species, although this is particularly variable in *Gorilla*; this can be seen in Figure 3, where the scores of apes along PC2 are largely driven by this feature.

<u>*Australopithecus anamensis*</u> This is the earliest hominin species in our sample, which is reflected in a number of symplesiomorphic features of the crown shape, including weak development of the mesial marginal ridge, and a mesiobuccal extension of the CEJ. The CEJ is not lowered on the mesiobuccal side as in apes, which means the characteristic sinusoidal shape is not present. The transverse crest extends to meet the marginal ridge on the lingual side of the crown, causing the marginal ridge to be raised at this point, relative to the condition seen in *Pan, Gorilla*, and *Hylobates*.

<u>*Australopithecus afarensis*</u> The *A. afarensis* hypodigm is variable, with some specimens more similar to *A. anamensis* than others; the two taxa are found not to differ significantly from each other in shape ($p = 0.133$) or size ($p = 0.585$). Specimens such as A.L. 128-23 and A.L. 266-1 display little mesial marginal ridge development and no metaconid, similar to *A. anamensis,* whilst others, such as A.L. 333w-1c, display a well-developed metaconid and mesial marginal ridge, similar to later *Australopithecus* and *Paranthropus* specimens. The Pliocene specimens from the Omo-Turkana region, W8-978 and KNM-WT 8556, also both display a well-developed mesial marginal ridge and a clear metaconid. In the mean wireframe model (Fig. 2), the *A. afarensis* metaconid is more mesially placed than in *A. anamensis*,

reducing the size of the mesial fovea. At the OES, a longitudinal groove is variably present, which at the EDJ appears to derive from the presence of a well-developed metaconid that is well separated from the protoconid, as well as a lowered, convex transverse crest. This combination of features can be seen in A.L. 333w-1c and its antimere, as well as potential *A. afarensis* specimens KNM-WT 8556 and W8-978. *Australopithecus afarensis* also has a taller crown than *A. anamensis*, which is particularly marked on the mesial side, and is associated with the development of the mesial marginal ridge in some specimens. The CEJ is raised on the mesial and distal sides, which is characteristic of *Australopithecus* and *Paranthropus* species (except *A. anamensis*), and is also seen in *H. naledi.* This is generally more prominent on the mesial side, particularly in *P. robustus,* in which the mesial side of the CEJ shows a marked upward protrusion.

<u>*Australopithecus africanus*</u> In terms of centroid size, *A. africanus* specimens overlap greatly with specimens of *A. afarensis*, and the two species were not significantly different in the size permutation test (p = 0.473). In fact, size alone is not useful in distinguishing the P_3 of *Australopithecus* species (Table 2). The *A. africanus* sample substantially overlaps with *A. afarensis* in shape space in the EDJ+CEJ and CEJ only analyses (Fig. 3; SOM Fig. S2). However, when only the EDJ is considered, the two species are mostly separated (Fig. 4).

In the mean wireframe models, the *A. africanus* mesial fovea is buccolingually wider than earlier *Australopithecus,* and the metaconid is placed more lingually. The mesial marginal ridge is relatively lower in *A. africanus* than *A. afarensis*, which likely reflects that in some specimens (e.g., STW 213, STW 401) the ridge is interrupted mesial to the metaconid. Compared to *A. anamensis* and *A. afarensis*, the CEJ is buccolingually wider and, as in earlier *Australopithecus*, is raised on the lingual and distal sides.

STW 213 is separated from the other *A. africanus* specimens in the EDJ+CEJ analysis in PC2 (Fig. 3). In this specimen, the distal marginal ridge appears 'pinched' distal to the metaconid, and is interrupted on the lingual side, only beginning again at on the lingual margin of the tooth. The specimen is also the smallest of the *A. africanus* sample (in fact, it is the smallest *Australopithecus* specimen in the EDJ+CEJ sample), and has a particularly tall protoconid. Buccal ridges, common in the *A. africanus* hypodigm, are especially prominent in this specimen, as is a distobuccal accessory cusp. In the CVA classifications, the specimen is often misclassified as *A. afarensis*, or occasionally as *H. naledi*, and this is more common in the form analysis than the shape analysis, underlining the contribution of the small size.

<u>*Paranthropus*</u> Although the mean centroid size of *P. robustus* is the largest of any hominin species included here (excluding *Paranthropus boisei*, for which only two specimens were able to be included in the EDJ+CEJ analysis), there is significant overlap with other hominin taxa, and we failed to find a significant difference between the size of *P. robustus* and any *Australopithecus* species (Table 2). *Paranthropus robustus* displays a distal fovea that is larger than that of *Australopithecus* specimens due to an expansion of the talonid region, as well as shifting of the metaconid mesially, which leads to the transverse crest projecting mesiolingually from the protoconid, as opposed to *Australopithecus* specimens in which the transverse crest is angled more lingually. The CEJ is expanded, particularly on the buccal side, which leads to a more squared buccal face. *Paranthropus robustus* specimens display a raised section of the CEJ on the mesial side which begins at the mesiobuccal corner of the tooth and ends just beyond the midpoint of the mesial face of the tooth. In general, *A. afarensis* and *A. africanus* specimens also display CEJs that are raised on the mesial side, although the condition in *P. robustus* is more pronounced.

In the EDJ+CEJ analysis, *P. robustus* specimens occupy a large area across PC3, with Drimolen specimens on one extreme and Swartkrans specimens on the other (Fig. 3),

363 suggesting there may be distinct shape differences between the two sites. The two Drimolen
364 specimens in the CEJ+EDJ analysis display an EDJ ridge that is larger, relative to the size of
365 the CEJ, than the Swartkrans specimens in this analysis, as well as a relatively lower dentine
366 body height. However, since this is only based on two Drimolen and three Swartkrans
367 specimens, this pattern requires further investigation. Only two *P. boisei* specimens were
368 included in the EDJ+CEJ analysis; however, they occupy a distinct space in Figure 3, largely
369 due to a talonid that is enlarged even relative to *P. robustus.*

370 Early *Homo* specimens Wireframe models for two early *Homo* specimens are presented in
371 Figure 6. SKX 21204 has a number of derived features relative to *Australopithecus*. The
372 crown is tall, the metaconid is reduced, and the talonid is small. Compared to *A. afarensis* and
373 *A. africanus*, it has a flatter, more oval CEJ. The specimen is also very small; the centroid
374 size is within the range of modern *H. sapiens*. KNM-ER 992 is larger, with a centroid size
375 within the range of *P. robustus*, and close to the largest *A. afarensis* and *H. neanderthalensis*
376 specimens. As in SKX 21204, the metaconid is smaller than the majority of *A. africanus*
377 specimens, and more distally placed. The talonid is also relatively small. However, in both
378 the EDJ+CEJ and the EDJ only analyses, the specimen falls close to the *A. africanus* range of
379 variation (Figs. 3 and 4).

380 A number of early *Homo* specimens could only be included in the CEJ only analysis. The
381 main distinguishing feature of the CEJ is the transition from an asymmetrical shape when
382 viewed occlusally (with a mesiobuccal expansion) in earlier hominin taxa, mostly
383 *Australopithecus*, to a roughly oval CEJ in modern humans and Neanderthals. This is evident
384 in the placement of a number of African early *Homo* specimens in the PCA of the CEJ only
385 analysis (SOM Fig. S2). Kenyan specimens KNM-ER 992A, KNM-ER 806E, and KNM-WT
386 15000B, as well as Swartkrans specimen SKX 21204, are clearly distinct from the

387 *Australopithecus* and *Paranthropus* clusters, while KNM-ER 1507 and SK 18a sit at the
388 periphery of the range of these groups.

389 <u>*Homo naledi*</u> In shape space, the *H. naledi* P_3 occupies a distinct area in all except the CEJ
390 only analysis (SOM Fig S2). They occupy the lower end of the size range of *H.*
391 *neanderthalensis* (Fig. 5), and are smaller than most *Australopithecus* specimens. In size,
392 they significantly differ from all other taxa included here (Table 2), and in shape they are
393 significantly different from all except *P. robustus* (Table 3). One of the most striking features
394 of the *H. naledi* P_3 is the metaconid, which is uniformly well developed, and only marginally
395 shorter than the protoconid. Compared to *Australopithecus* specimens, the crown is higher,
396 especially on the mesial side, with a well-developed mesial marginal ridge. The talonid
397 region is reduced compared to *P. robustus*, leading to an EDJ ridge that is more symmetrical
398 in occlusal view (Fig. 2). The CEJ is relatively narrower buccolingually than
399 *Australopithecus* specimens, and the buccal face is flattened, as is seen in *P. robustus,* and, to
400 an extent, *A. afarensis*. The *H. naledi* CEJ resembles the condition seen in *Australopithecus*
401 and *Paranthropus* more than the modern human and Neanderthal condition as there are no
402 signs of the derived oval shape, and the mesial side is raised as in *Australopithecus*. In
403 Figures 3 and 4, *H. naledi* specimens cluster closely together.

404 <u>Modern humans and Neanderthals</u> Modern humans and Neanderthals display an oval CEJ
405 when viewed occlusally. The distal fovea is reduced in size through reduction of the talonid
406 region, when compared with earlier hominins in the sample. They also have a tall dentine
407 body height, a tall protoconid with tall mesial and distal protoconid crests, and reduced
408 metaconid development. This morphology can also be seen in fossil modern humans from
409 Qafzeh and the Cave of Hearths P_3, which is of uncertain taxonomic affinity. Although the
410 Mauer P_3 is too worn to include in analyses considering the entire EDJ ridge, the preserved
411 EDJ morphology strongly suggests that it fits the modern human and Neanderthal condition.

Modern humans and Neanderthals are separated from each other in the EDJ+CEJ analysis (Fig. 3). This separation mainly pertains to the shape of the EDJ ridge. Neanderthals frequently display a transverse crest which intersects with the marginal ridge more distally than in recent modern humans. The Neanderthal EDJ ridge is relatively longer mesiodistally, whilst the modern human EDJ ridge is mesiodistally shortened, and therefore more circular. Neanderthal specimens frequently display a protoconid tip which protrudes lingually, towards the centre of the tooth, a feature which is much less common in modern humans. Also, the wireframe models show that the Neanderthal CEJ is flattened apicocervically, whereas the modern human CEJ is lowered on the buccal side, and raised on the mesial and distal sides (Fig. 2). This is not present in all modern human specimens, and can sometimes be seen in Neanderthal specimens, but the differences in frequency are enough for this to be picked up in the wireframe models. Further, the two Qafzeh specimens more closely approximate the modern human condition. The P_3 in Neanderthals is larger than that of modern *H. sapiens* ($p = 0.002$, Fig. 5).

3.2 Classification accuracies

The CVA classification accuracies are summarized in Table 4; accuracies are reported for each of the GM analyses. Classification results for each specimen individually can be found in SOM Table S3. The best performing analysis overall was the EDJ+CEJ analysis (88%), closely followed by the EDJ only analysis (87%). The CEJ only analysis performed poorest overall (69%), but was improved by the inclusion of the metaconid landmark (80%).

3.3 Specimens of uncertain taxonomic affinity

The P_3 of KNM-WT 8556 does not fall within the variation of our sample of Hadar *A. afarensis*, or any other taxon, in the EDJ+CEJ or EDJ only analyses. W8-978 is within the *A. afarensis* cluster, and close to the *A. africanus* cluster, in the EDJ+CEJ analysis (Fig. 3), and in the EDJ only analysis, it is close to *A. africanus* , but separated from *A. afarensis* in PC3 (this is not visible in Fig. 4 due to the orientation of the plot). Similarly, KNM-ER 5431E does not fall within the variation of any of our groups, although in the EDJ only analysis, which better distinguishes between *A. afarensis* and *A. africanus* (Fig. 4 and SOM Table S3), the specimen plots more closely to *A. africanus*. While STW 151 falls close to the *A. africanus* range of variation in the EDJ only analysis (Fig. 4), the specimen plots far from all other specimens in the EDJ+CEJ analysis (Fig. 3). This is likely due to the particularly low dentine body height of this specimen when compared with other *A. africanus* specimens, a factor which is not represented in the EDJ only analysis. The Cave of Hearths P_3 has a morphology similar to that of Neanderthals (Figs. 3 and 4).

4. Discussion

4.1 Premolar morphology for taxonomy

As expected, the highest classification accuracies of the known taxonomic sample were in the analyses that included both the EDJ marginal ridge and the cervix (Table 4), suggesting that incorporation of shape information that includes dentine horn height and spacing, the shape of the occlusal basin, the height of the crown and the shape of the cervix provides the most accurate method of assessing questions of taxonomy. The EDJ only analysis performs nearly as well; although this analysis contains less shape information, the sample sizes are larger and it is likely that this allows more accurate classifications for some specimens (particularly Plio-Pleistocene hominins). The CEJ only analyses did not perform as well, and

although the addition of the metaconid landmark improved the classification accuracy, both performed poorly at differentiating Plio-Pleistocene hominins (SOM Table S3). Ultimately, analyses relying largely on the cervix shape are sufficient for distinguishing among hominoid genera, and perform reasonably well at distinguishing between modern humans and Neanderthals. However, for distinguishing among Plio-Pleistocene hominin species, including the EDJ ridge is most appropriate.

4.2 Specimens of uncertain taxonomic affinity

The mandible fragment KNM-WT 8556 has previously been attributed to *A. afarensis* (Brown et al., 2001) and is found in the same Lomekwi locality as specimens attributed to *K. platyops* (Leakey et al., 2001). Here, the specimen does not closely cluster with *A. afarensis*, although the *A. afarensis* hypodigm is morphologically variable (Leonard and Hegmon, 1987; Suwa, 1990), especially in P_3 morphology (Delezene and Kimbel, 2011), and it is very likely that not all of this variation is covered in our sample of Hadar *A. afarensis*. Regardless, until we have a larger sample of dental specimens that are clearly attributable to *K. platyops*, the taxonomic affinities of KNM-WT 8556 will be difficult to resolve. W8-978, an isolated P_3 from the Usno Formation, Ethiopia, dated to 3.05 Ma (Feibel et al., 1989), has been variably included in *Australopithecus* sp. (Coppens, 1978), aff. *A. afarensis* (Suwa, 1990), *A. africanus* (Boaz, 1997), and *A. afarensis* (Leonard and Hegmon, 1987). Here, the specimen clusters with both *A. afarensis* and *A. africanus*. The P_3 of *Australopithecus deyiremeda* is described as displaying an asymmetrical crown and a combination of strong mesial but weak distal buccal grooves (Haile-Selassie et al., 2015), both of which are present in W8-978. However these features are common in early *Australopithecus* P_3 and, moreover, the *A. deyiremeda* P_3 is also described as having a minimally developed metaconid, unlike W8-978 where the metaconid is reasonably well-developed. Future examination of the dentine crown of *A. deyiremeda* would be helpful in assessing the taxonomic affinity of W8-978.

KNM-ER 5431 consists of a set of associated mandibular teeth that have previously been assigned to *A. afarensis* (Leonard and Hegmon, 1987), whilst Suwa (1990) suggested that the premolar morphology of the specimen was derived relative to *A. afarensis,* and instead assigned it to '*Australopithecus*/*Homo* gen. and sp. indet'. Similarly, Wood (1991) suggested that the molars of the specimen show similarities to those of early *Homo,* but did not assign the specimen to a species. Here, the left P_3 (KNM-ER 5431E) groups with the *A. africanus* and *A. afarensis* specimens in the EDJ+CEJ analysis, although it also falls close to some African early *Homo* specimens. The early *Homo* sample in this analysis is relatively fragmentary, so for specimens such as this one, a sample of *Homo habilis* would be required for a full comparison. This specimen also shows a relatively small metaconid, as is described for the P_3 of *A. deyiremeda*. However, the inclusion of all available tooth positions in the KNM-ER 5431 sample is required to confidently assess its taxonomic affinities.

STW 151 represents a number of cranial and dental fragments of a juvenile individual from Sterkfontein and was suggested by Moggi-Cecchi et al. (1998) to display a number of derived features compared with other Sterkfontein *A. africanus*. In terms of discrete traits, the P_3 was said to lack any derived early *Homo* traits, but the shape clustered with the smaller *A. africanus* specimens, towards the range of *H. habilis*. Our analysis of the P_3 does not contradict this assessment, with the specimen falling outside of the *A. africanus* range of variation, particularly in the EDJ+CEJ analysis (Fig. 3). The specimen does not cluster closely with other early *Homo* specimens; however, a larger early *Homo* sample, including *H. habilis*, would be required to fully assess the affinities of this specimen.

The Cave of Hearths mandible is from Makapansgat, South Africa, and was found in a layer with late Achulean industry tools. In the original description, and later analyses, similarities with Neanderthals were noted (Dart, 1948; Tobias, 1971) and this is mirrored in our results here. In the EDJ+CEJ analysis, the specimen falls close to, but not within, the

Neanderthal range of shape variation (Fig. 3). This could suggest that on the basis of P_3 morphology, the Cave of Hearths mandible likely represents Middle- or Late-Pleistocene *Homo*, which is distinct from *H. sapiens*. Berger et al. (2017) raised the possibility that the Cave of Hearths specimen may represent *H. naledi*, but this is not supported in our analysis; the Cave of Hearths P_3 is clearly separated from those of *H. naledi*, and lacks a number of very distinctive *H. naledi* P_3 features. Future analyses should compare this specimen to other African later Pleistocene mandibular specimens such as those from Jebel Irhoud and Thomas Quarry.

4.3 Major EDJ shape trends

<u>Canine honing</u> The observed P_3 morphology of the extant apes is driven largely by its function in the honing complex. This explains the presence of the tall projecting protoconid and the apical extension of the cervix on the mesiobuccal side. Since the cervix marks the limit of the tooth's enamel coverage, the cervix likely extends further apically to provide an apicocervically long (as well as mesiodistally broad) sloping surface along which the upper canine can occlude. This apical extension is not seen in the earliest hominin in our sample, *A. anamensis*, having been presumably lost alongside, or after, the loss of the canine honing complex. However, other features relating to honing can be found in hominins, such as the tall protoconid and poor development of both the metaconid and mesial marginal ridge seen in *A. anamensis* (Ward et al., 2001; Delezene and Kimbel, 2011). Moreover, the P_3 in *Australopithecus* displays a mesiobuccally expanded cervix (Fig. 2). This feature is clearest in *A. anamensis*, although it is far less pronounced than in the extant apes.

<u>Cervix morphology</u> The P_3 occlusal outline, or occlusal crown shape, has been discussed extensively for fossil hominin teeth, and refers to the 2D shape of the tooth in occlusal view

533 (Wood and Uytterschaut, 1987; Asfaw et al., 1999; Bailey and Lynch, 2005; Martinón-Torres
534 et al., 2006; Gómez-Robles et al., 2008). Assessed essentially as a 2D occlusal projection,
535 this trait is related to the shape of the cervix in occlusal view, although they are not exactly
536 the same since the occlusal crown shape pertains to the outward-most protrusion of the
537 enamel crown on all sides. It has been suggested that the occlusal outline is a poor taxonomic
538 discriminator since it is variable within a number of taxa (Strait et al., 1997). However
539 another related trait, the mesiobuccal protrusion of the crown base, is thought to have better
540 discriminatory power (White et al., 1994; Strait and Grine, 2004). Here, we find a large
541 degree of intraspecific variation in cervix shape within Plio-Pleistocene hominins (SOM Fig.
542 S2), as well as relatively low classification accuracy in the CEJ only analysis (Table 4).
543 Broad patterns can be observed; apes typically have a cervix which is strongly asymmetrical
544 in occlusal view due to an enlarged mesiobuccal component associated with canine honing
545 (Fig. 2), early hominins display a more symmetrical cervix with the loss of canine honing,
546 while modern humans and Neanderthals have a more symmetrical, oval cervix which is
547 shared with some early *Homo* specimens (Fig. 6).

548 The shape of the cervix is partly dependent on root formation, and it is likely that the
549 single roots of the modern human and Neanderthal P_3 (Cleghorn et al., 2007; Shields, 2015)
550 contribute to the oval shape. Earlier hominins, meanwhile, display a larger range of root
551 morphologies: *A. africanus* and *P. robustus* have highly variable root morphologies (Moore
552 et al., 2016), while *H. naledi* P_3 are typically double-rooted (Berger et al., 2015), and the *A.*
553 *afarensis* P_3 can be single or double rooted (Ward et al., 1982). Another feature seen in a
554 number of hominin species, in which the cervix is raised on the mesial and/or distal sides,
555 also appears to be related to root structure as the cervix curves over the base of the roots,
556 sitting highest on the tooth crown when in line with the middle of the base of the root, and
557 lowest when in line with interradicular grooves.

558 <u>*A. anamensis to A. afarensis*</u> *Australopithecus anamensis* is hypothesized to be the direct
559 ancestor of *A. afarensis*, with the two species possibly representing an anagenetic lineage
560 (Ward et al., 1999; Kimbel et al., 2006, White et al., 2006; Haile-Selassie et al., 2010). Our
561 sample only included *A. anamensis* specimens from ~4.2 Ma deposits at Kanapoi and *A.*
562 *afarensis* specimens mostly from Hadar at ~3.2 Ma (Johanson et al., 1982; Walter, 1994;
563 Leakey et al., 1998), meaning there is a 1 Myr gap between the samples. Only *A. anamensis*
564 specimen KNM- KP 53160 clusters closely with the *A. afarensis* sample in the EDJ+CEJ
565 analysis (Fig. 3), and given that this is not the case in the EDJ only analysis (Fig. 4), it is
566 likely that this is mostly due to the slightly taller dentine body in KNM-KP 53160, compared
567 with KNM-KP 29281 and KNM-KP 29286. Ward et al. (2017) also noted that the P_4 of
568 KNM-KP 53160 had a particularly large distal fovea, closer to the range of *A. afarensis* than
569 *A. anamensis*. However, the overall dental morphology of the specimen is still very similar to
570 other Kanapoi *A. anamensis* specimens (Ward et al., 2017). In order to better assess this
571 hypothesis using our method, a larger and more comprehensive sample from other sites
572 would be required. Particularly important for this discussion are younger *A. anamensis*
573 specimens from Allia Bay (3.9 Ma) and Woranso-Mille (3.6–3.8 Ma), both of which have
574 been described as showing features more similar to that of *A. afarensis* (Delezene and
575 Kimbel, 2011; Deino et al., 2010; Haile-Selassie, 2010; Haile-Selassie et al., 2010)

576 *Australopithecus afarensis* has a particularly variable hypodigm; for the P_3, crown size,
577 metaconid expression, and mesial marginal ridge development are all variable, often
578 independently of one another, and these features even vary within the same site (Leonard and
579 Hegmon, 1987; Suwa, 1990; Delezene and Kimbel, 2011). Here, we failed to find a
580 significant difference in size or shape between *A. afarensis* and either *A. anamensis* or *A.*
581 *africanus*, and it is likely that this variability, as well as small sample sizes, is the reason for
582 this. Two *A. afarensis* specimens, both from Hadar, are shown in Figure 7, demonstrating

583 some of the variation in the taxon even within a site. Despite this variability, it is clear that a
584 number of the features common in later hominins, such as *A. africanus* and *P. robustus*
585 (including a well-developed metaconid, an increase in talonid size, and a well-developed
586 mesial marginal ridge), do appear first in *A. afarensis*. In our sample, *A. afarensis* is
587 represented by specimens from Hadar, although many of these derived features are also
588 variably present in earlier specimens from Laetoli (Delezene and Kimbel, 2011). It would
589 also be interesting to compare the EDJ morphology of these specimens to that of *A.*
590 *deyiremeda*. The species is described as showing some derived features relative to *A.*
591 *afarensis,* although the P_3 of the paratype BRT-VP-3/14 is described as being nearly
592 unicuspid, with a poorly defined mesial marginal ridge, as is seen in *A. anamensis* and some,
593 but not all, *A. afarensis* specimens.

594 Mastication and molarization A number of EDJ features point to increasing masticatory
595 demands on the P_3 in some of the study taxa. As noted above, specimens of *A. afarensis* are
596 the first to display a well-developed metaconid and a well-developed mesial marginal ridge,
597 enclosing the occlusal area. These features are more common in *A. africanus,* and ubiquitous
598 in *P. robustus*. A similar pattern is seen in the expansion of the talonid; *A. afarensis* and *A.*
599 *africanus* show expanded talonids when compared with apes and *A. anamensis*, but this
600 feature is most clearly seen in *Paranthropus*. The wireframe models in Figure 2 show a large
601 talonid in *P. robustus*, and this plays a role in the separation of *P. robustus* from
602 *Australopithecus* taxa in Figures 3 and 7. Unfortunately, for the majority of specimens of *P.*
603 *boisei* (considered the most derived with respect to the masticatory changes observed in
604 *Paranthropus*) the CT scans exhibit little or no contrast between tissue types (for an example
605 of a low contrast scan, see SOM Fig. S1), preventing detailed examination of the EDJ
606 surface. However, the few specimens for which the EDJ morphology was visible did show
607 strong talonid development. Two further features relating to mastication and molarization, the

enclosure of the P_3 marginal ridges, and the presence of accessory cusps, are discussed in a companion paper on discrete traits (Davies et al., under review).

Early *Homo* The conclusions of this study with respect to earlier members of the genus *Homo* are limited due to a limited sample. However, there are some specimens which can be discussed. KNM-ER 992 is thought to be closely aligned with African *H. erectus* (Howell, 1978; Wood, 1991), and was used by Groves and Mazák (1975) as the holotype of *H. ergaster*. Relative to most *Australopithecus* and *Paranthropus*, the P_3 displays a reduced talonid, a short metaconid and a flattened, oval CEJ. Wood (1991) noted a number of similarities between this specimen and *A. africanus* mandibles, which is reflected in our GM analysis.

SKX 21204 is from Swartkrans Member 1 and was attributed to *Homo* on the basis of a number of dental and mandibular features (Grine, 1989), although not on the basis of the P_3, which is unerupted. The EDJ surface morphology of the specimen was analyzed by Pan *et al.* (2016), where they found the P_3 to be within the modern human range of variation, and the P_4 to be intermediate between modern humans, *A. africanus*, and *P. robustus*. Here, the P_3 is found to display a number of derived features relative to *Australopithecus* specimens, although it is also clearly distinct from modern humans. This is largely due to the relatively short dentine body height, which appears to be one of the main drivers of the separation of earlier hominins from modern humans and Neanderthals. This can be seen in SOM Figure S3, where SKX 21204 is closest to the range of *H. naledi*, followed by *P. robustus*. However, in Figs. 3 and 4 the specimen does not cluster with *H. naledi*, and the centroid size of the specimen is much smaller than that of *P. robustus* specimens. The CEJ morphology of the specimen is similar to *H. ergaster* specimens KNM-WT 15000, KNM-ER 992 and KNM-ER 806E (SOM Fig. S2).

Later *Homo* Modern humans, despite their variability, can be characterized as displaying a tall dentine body, a reduced metaconid, and tall protoconid crests, a morphology which is also seen in Neanderthals, Mauer, and Cave of Hearths. Whilst these aspects of P_3 morphology mirror that seen in apes and *A. anamensis*, the overall shape of the crown is very different. Modern human and Neanderthal specimens are most clearly distinguished by an increase in dentine body height compared with earlier hominins.

Despite its Middle Pleistocene age (Dirks et al., 2017), *H. naledi* is found to be clearly distinct from modern humans and Neanderthals, as well as from Mauer and Cave of Hearths. The morphology more closely resembles that of *A. africanus*, *P. robustus* or specimens of early *Homo* (SOM Fig. S3)*;* however, none of these groups display the combination of features seen in *H. naledi*, and the EDJ shape of the species is clearly distinct (Figs. 3 and 4). Analysis of the EDJ of other tooth positions of *H. naledi*, as well as a wider comparative sample, may help shed further light on the relationships between *H. naledi* and other hominin taxa.

5. Conclusions

This study adds to a growing body of evidence suggesting that mandibular third premolars hold a wealth of taxonomically important information, and that geometric morphometric analysis of P_3 EDJ shape and size can be used in reliably assigning specimens to well-accepted taxonomic groups. This could be useful in taxonomic identification of isolated specimens, although as shown here in the case of KNM-WT 8556, this is dependent on the available comparative sample.

Apes have a P_3 morphology which is specialized for its role in honing the large upper canine. Wireframe models show a tall crown, and a mesiobuccally expanded CEJ which is

lowered, apically, in order to provide a long, broad sloping surface for the upper canine. Early hominin evolution can be characterized by the gradual loss of features relating to canine honing, particularly the reduction of both the protoconid and the mesiobuccal extent of the CEJ. Moreover, we see the gradual accumulation of features related to improved masticatory abilities such as the enclosing of the occlusal surface of the tooth through the stronger development the mesial marginal ridge, the development of a large metaconid, and the expansion of the talonid. The earliest members of *Homo* appear to have a morphology largely similar to that of a number of *Australopithecus* specimens, although there are differences, which require further investigation though looking at the EDJ of a larger sample of early *Homo* specimens. *Homo naledi* displays a morphology that is unique among this sample, but appears surprisingly primitive for a species of *Homo* given the age of the material, displaying a well-developed metaconid, strong mesial and distal marginal ridges, and an asymmetrical CEJ. Modern humans and Neanderthals have a distinctive morphology including a tall dentine body and a reduced metaconid. The morphology of the P_3 in these taxa likely reflects the altered dietary adaptations in late *Homo* species related to their increased geographical range, differing climates, and increased dietary specializations.

Studies of the EDJ in fossil hominins remain hugely important in improving the amount of morphological information which can be gained from worn dental specimens, allowing the study of larger samples and the utilisation of as much fossil material as possible.

References

Anemone, R.L., Skinner, M.M., Dirks, W., 2012. Are there two distinct types of hypocone in Eocene primates? The ‘pseudohypocone’of notharctines revisited. Palaeontologia Electronica 15, 26A.

Asfaw, B., White, T., Lovejoy, O., Latimer, B., Simpson, S., Suwa, G., 1999. *Australopithecus garhi*: a new species of early hominid from Ethiopia. Science 284, 629-635.

Bailey, S.E., Lynch, J.M., 2005. Diagnostic differences in mandibular P4 shape between Neandertals and anatomically modern humans. American Journal of Physical Anthropology 126, 268-277.

Benjamini, Y. and Hochberg, Y., 1995. Controlling the false discovery rate: a practical and powerful approach to multiple testing. Journal of the Royal Statistical Society B 57, 289-300.

Berger, L.R., Hawks, J., de Ruiter, D.J., Churchill, S.E., Schmid, P., Delezene, L.K., Kivell, T.L., Garvin, H.M., Williams, S.A., DeSilva, J.M., Skinner, M.M., Musiba, C.M., Cameron, N., Holliday, T.W., Harcourt-Smith, W., Ackermann, R.R., Bastir, M., Bogin, B., Bolter, D., Brophy, J., Cofran, Z.D., Congdon, K.A., Deane, A.S., Dembo, M., Drapeau, M., Elliott, M.C., Feuerriegel, E.M., Garcia-Martinez, D., Green, D.J., Gurtov, A., Irish, J.D., Kruger, A., Laird, M.F., Marchi, D., Meyer, M.R., Nalla, S., Negash, E.W., Orr, C.M., Radovčić, D., Schroeder, L., Scott, J.E., Throckmorton, Z., Tocheri, M.W., Vansickle, C., Walker, C.S., Wei, P., Zipfel, B., 2015. *Homo naledi*, a new species of the genus *Homo* from the Dinaledi Chamber, South Africa. eLife 4, e09560.

Beynon, A.D., Wood, B.A., 1986. Variations in enamel thickness and structure in East African hominids. American Journal of Physical Anthropology 70, 177-193.

Boaz, N.T., 1977. Paleoecology of Plio-Pleistocene Hominidae in the lower Omo basin, Ethiopia. Ph.D. Dissertation, University of California.

Bookstein, F.L., 1997. Landmark methods for forms without landmarks: morphometrics of group differences in outline shape. Medical Image Analysis 1, 225-243.

Braga, J., Thackeray, J.F., Subsol, G., Kahn, J.L., Maret, D., Treil, J., Beck, A. 2010. The enamel–dentine junction in the postcanine dentition of *Australopithecus africanus*: intra-individual metameric and antimeric variation. Journal of Anatomy 216, 62-79.

Brown, B., Brown, F.H., Walker, A., 2001. New hominids from the Lake Turkana basin, Kenya. Journal of Human Evolution 41, 29-44.

Brunet, M., Guy, F., Pilbeam, D., Mackaye, H.T., Likius, A., Ahounta, D., Beauvilain, A., Blondel, C., Bocherens, H., Boisserie, J. De Bonis, L., Coppens, Y., Dejax, J., Denys, C., Duringer, P., Eisenmann, V., Fanone, G., Fronty, P., Geraads, D., Lehmann, T., Lihoreau, F., Louchart, A., Mahamat, A., Merceron, G., Mouchelin, G., Otero, O., Campomanes, P.P., De Leon, M.P., Rage, J., Sapanet, M., Schuster, M., Sudre, J., Tassy, P., Valentin, X., Vignaud, P., Viriot, L., Zazzo, A., Zollikofer, C., 2002. A new hominid from the Upper Miocene of Chad, Central Africa. Nature 418, 145-151.

Carayon, D., Adhikari, K., Monsarrat, P., Dumoncel, J., Braga, J., Duployer, B., Delgado, M., Fuentes-Guajardo, M., de Beer, F., Hoffman, J.W., Oettlé, A.C., 2019. A geometric morphometric approach to the study of variation of shovel-shaped incisors. American Journal of Physical Anthropology 168, 229-241.

Cleghorn, B.M., Christie, W.H., Dong, C.C., 2007. The root and root canal morphology of the human mandibular first premolar: a literature review. Journal of Endodontics 33, 509-516.

Conroy, G.C., 1991. Enamel thickness in South African australopithecines: noninvasive evaluation by computed tomography. Palaeontologica Africana 28, 53-59

Coppens, Y., 1980. The differences between *Australopithecus* and *Homo*: preliminary conclusion from the Omo Research Expedition's studies. In: Konigsson, L.K. (Ed.), Current Argument on Early Man. Pergamon Press, New York, pp. 207-225.

Dart, R.A., 1948. The first human mandible from the Cave of Hearths, Makapansgat. The South African Archaeological Bulletin 3, 96-98.

Deino, A.L., Scott, G.R., Saylor, B., Alene, M., Angelini, J.D., Haile-Selassie, Y. 2010. $^{40}Ar/^{39}Ar$ dating, paleomagnetism, and tephrochemistry of Pliocene strata of the hominid-bearing Woranso-Mille area, west-central Afar Rift, Ethiopia. Journal of Human Evolution 58, 111-126.

Delezene, L.K., 2015. Modularity of the anthropoid dentition: Implications for the evolution of the hominin canine honing complex. Journal of Human Evolution 86, 1-12.

Delezene, L.K., Kimbel, W.H., 2011. Evolution of the mandibular third premolar crown in early *Australopithecus*. Journal of Human Evolution 60, 711-730.

Dirks, P.H., Roberts, E.M., Hilbert-Wolf, H., Kramers, J.D., Hawks, J., Dosseto, A., Duval, M., Elliott, M., Evans, M., Grün, R., Hellstrom, J., 2017. The age of *Homo naledi* and associated sediments in the Rising Star Cave, South Africa. eLife 6, e24231.

Dryden, I., Mardia, K.V., 1998. Statistical Shape Analysis. John Wiley and Sons, New York.

Feibel, C.S., Brown, F.H., McDougall, I., 1989. Stratigraphic context of fossil hominids from the Omo Group deposits: northern Turkana Basin, Kenya and Ethiopia. American Journal of Physical Anthropology 78, 595-622.

Goodall, C., 1991. Procrustes methods in the statistical analysis of shape. Journal of the Royal Statistical Society B 53, 285-339

Gómez-Robles, A., Martinón-Torres, M., Bermúdez de Castro, J.M., Prado, L., Sarmiento, S., Arsuaga, J.L., 2008. Geometric morphometric analysis of the crown morphology of the lower first premolar of hominins, with special attention to Pleistocene *Homo*. Journal of Human Evolution 55*,* 627-638.

Grine, F.E., 1986. Dental evidence for dietary differences in *Australopithecus* and *Paranthropus*: a quantitative analysis of permanent molar microwear. Journal of Human Evolution 15, 783-822.

Grine, F.E., 1989. New hominid fossils from the Swartkrans Formation (1979–1986 excavations): craniodental specimens. American Journal of Physical Anthropology 79, 409-449.

Grine, F.E., Martin, L., 1988. Enamel thickness and development in *Australopithecus* and *Paranthropus*. In: Grine, F.E. (Ed.), Evolutionary History of the “Robust” Australopithecines. Aldine de Gruyter, New York, pp. 3-42.

Grine, F.E., Sponheimer, M., Ungar, P.S., Lee-Thorp, J., Teaford, M.F., 2012. Dental microwear and stable isotopes inform the paleoecology of extinct hominins. American Journal of Physical Anthropology 148, 285-317.

Groves, C.P., Mazák, V. 1975. An approach to the taxonomy of the Hominidae: gracile Villafranchian hominids of Africa. Casopis Pro Mineralogii a Geologii 20, 225–247

Gunz, P., Mitteroecker, P., 2013. Semilandmarks: a method for quantifying curves and surfaces. Hystrix 24, 103-109.

Gunz, P., Mitteroecker, P., Bookstein, F., 2005. Semilandmarks in three dimensions. In: Slice, D.E. (Ed.), Modern Morphometrics in Physical Anthropology. Kluwer Academic/Plenum Publishers, New York, pp. 73-98.

Guy, F., Lazzari, V., Gilissen, E., Thiery, G., 2015. To what extent is primate second molar enamel occlusal morphology shaped by the enamel-dentine junction? PLoS One 10, e0138802.

Haile-Selassie, Y. 2010. Phylogeny of early *Australopithecus*: new fossil evidence from the Woranso-Mille (central Afar, Ethiopia). Philosophical Transactions of the Royal Society B 365, 3323-3331.

Haile-Selassie, Y., Suwa, G., White, T.D. 2004. Late Miocene teeth from Middle Awash, Ethiopia, and early hominid dental evolution. Science 303, 1503-1505.

Haile-Selassie, Y., Saylor, B.Z., Deino, A., Alene, M., Latimer, B.M. 2010. New hominid fossils from Woranso-Mille (Central Afar, Ethiopia) and taxonomy of early *Australopithecus*. American Journal of Physical Anthropology 141, 406-417.

Haile-Selassie, Y., Gibert, L., Melillo, S.M., Ryan, T.M., Alene, M., Deino, A., Levin, N.E., Scott, G., Saylor, B.Z. 2015. New species from Ethiopia further expands Middle Pliocene hominin diversity. Nature 521, 483.

Hershkovitz, I., Weber, G.W., Quam, R., Duval, M., Grün, R., Kinsley, L., Ayalon, A., Bar-Matthews, M., Valladas, H., Mercier, N., Arsuaga, J.L. 2018. The earliest modern humans outside Africa. Science 359, 456-459.

Howell, F. C., 1978. Hominidae. In: Maglio, V.J, Cooke H.B.S. (Eds.), Evolution of African Mammals. Harvard University Press, Cambridge, pp. 154-248

Hublin, J.J., Ben-Ncer, A., Bailey, S.E., Freidline, S.E., Neubauer, S., Skinner, M.M., Bergmann, I., Le Cabec, A., Benazzi, S., Harvati, K., Gunz, P. 2017. New fossils from Jebel Irhoud, Morocco and the pan-African origin of *Homo sapiens*. Nature 546, 289-292.

Irish, J.D., Bailey, S.E., Guatelli-Steinberg, D., Delezene, L.K., Berger, L.R. 2018. Ancient teeth, phenetic affinities, and African hominins: Another look at where *Homo naledi* fits in. Journal of Human Evolution 122, 108-123.

Johanson, D.C., White, T.D. and Coppens, Y., 1978. A new species of the genus *Australopithecus* (Primates: Hominidae) from the Pliocene of East Africa. Kirtlandia 28, 1-14.

Johanson, D.C., White, T.D. and Coppens, Y., 1982. Dental remains from the Hadar Formation, Ethiopia: 1974–1977 collections. American Journal of Physical Anthropology 57, 545-603.

Kimbel, W.H., Lockwood, C.A., Ward, C.V., Leakey, M.G., Rak, Y., Johanson, D.C., 2006. Was *Australopithecus anamensis* ancestral to *A. afarensis*? A case of anagenesis in the hominin fossil record. Journal of Human Evolution 51, 134-152.

Kraus, B.S., Furr, M.L., 1953. Lower first premolars. Part I. A definition and classification of discrete morphologic traits. Journal of Dental Research 32, 554-564.

Le Gros Clark, W.E., 1967. Man-Apes or Ape-Men? The Story of Discoveries in Africa. Holt, Reinhard and Winston, New York.

Leakey, M.G., Feibel, C.S., McDougall, I., Walker, A. 1995. New four-million-year-old hominid species from Kanapoi and Allia Bay, Kenya. Nature 376, 565-571.

Leakey, M.G., Feibel, C.S., McDougall, I., Ward, C., Walker, A., 1998. New specimens and confirmation of an early age for *Australopithecus anamensis*. Nature 393, 62-66.

Leakey, M.G., Spoor, F., Brown, F.H., Gathogo, P.N., Kiarie, C., Leakey, L.N., McDougall, I., 2001. New hominin genus from eastern Africa shows diverse middle Pliocene lineages. Nature 410, 433-440.

Leonard, W.R., Hegmon, M., 1987. Evolution of P_3 morphology in *Australopithecus afarensis*. American Journal of Physical Anthropology 73*,* 41-63.

Martin, R.M., Hublin, J.-J., Gunz, P., Skinner, M.M., 2017. The morphology of the enamel–dentine junction in Neanderthal molars: Gross morphology, non-metric traits, and temporal trends. Journal of Human Evolution 103, 20-44.

Martinón-Torres, M., Bastir, M., Bermúdez de Castro, J.M., Gómez, A., Sarmiento, S., Muela, A., Arsuaga, J.L., 2006. Hominin lower second premolar morphology: evolutionary inferences through geometric morphometric analysis. Journal of Human Evolution 50*,* 523-533.

Moggi-Cecchi, J., Tobias, P.V., Beynon, A.D., 1998. The mixed dentition and associated skull fragments of a juvenile fossil hominid from Sterkfontein, South Africa. American Journal of Physical Anthropology 106, 425-465.

Moggi-Cecchi, J., Grine, F.E., Tobias, P.V., 2006. Early hominid dental remains from Members 4 and 5 of the Sterkfontein Formation (1966–1996 excavations): catalogue, individual associations, morphological descriptions and initial metrical analysis. Journal of Human Evolution 50, 239-328.

Molnar, S., 1971. Human tooth wear, tooth function and cultural variability. American Journal of Physical Anthropology 34, 175-189.

Morita, W., Yano, W., Nagaoka, T., Abe, M., Ohshima, H., Nakatsukasa, M., 2014. Patterns of morphological variation in enamel–dentin junction and outer enamel surface of human molars. Journal of Anatomy 224, 669-680.

Nager, G., 1960. Der Vergleich zwischen dem räumlichen Verhalten des Dentin-Kronenreliefs und dem Schmelzrelief der Zahnkrone. Cells Tissues Organs 42, 226-250.

Olejniczak, A.J., Smith, T.M., Skinner, M.M., Grine, F.E., Feeney, R.N.M., Thackeray, J.F., Hublin, J.-J., 2008. Three-dimensional molar enamel distribution and thickness in *Australopithecus* and *Paranthropus*. Biology Letters 4, 406-410.

Ortiz, A., Skinner, M.M., Bailey, S.E., Hublin, J.-J., 2012. Carabelli's trait revisited: An examination of mesiolingual features at the enamel–dentine junction and enamel surface of *Pan* and *Homo sapiens* upper molars. Journal of Human Evolution 63, 586-596.

Pan, L., Dumoncel, J., de Beer, F., Hoffman, J., Thackeray, J.F., Duployer, B., Tenailleau, C., Braga, J., 2016. Further morphological evidence on South African earliest *Homo* lower postcanine dentition: Enamel thickness and enamel dentine junction. Journal of Human Evolution 96, 82-96.

Pan, L., Thackeray, J.F., Dumoncel, J., Zanolli, C., Oettlé, A., de Beer, F., Hoffman, J., Duployer, B., Tenailleau, C., Braga, J., 2017. Intra-individual metameric variation expressed at the enamel-dentine junction of lower post-canine dentition of South African fossil hominins and modern humans. American Journal of Physical Anthropology 163, 806-815

R Core Team, 2018. R: A language and environment for statistical computing. R Foundation for Statistical Computing, Vienna

Robinson, J.T., 1956. The Dentition of the Australopithecinae. Transvaal Museum, Pretoria.

Rohlf, F.J., Slice, D., 1990. Extensions of the Procrustes method for the optimal superimposition of landmarks. Systematic Biology 39, 40-59.

Scott, G.R., Turner, C.G., 1997. Anthropology of Modern Human Teeth. Cambridge University Press, Cambridge

Sakai, T., 1967. Morphologic study of the dentinoenamel junction of the mandibular first premolar. Journal Dental Research 46, 927-932

Schulze, M.A., Pearce, J.A., 1994. A morphology-based filter structure for edge-enhancing smoothing. In: Proceedings of the 1st International Conference on Image Processing, IEEE Computer Society, Austin, pp. 530–534

Singleton, M., Rosenberger, A.L., Robinson, C., O'Neill, R., 2011. Allometric and metameric shape variation in *Pan* mandibular molars: A digital morphometric analysis. The Anatomical Record 294, 322-334.

Skinner, M.M., 2008. Enamel-dentine junction morphology of extant hominoid and fossil hominin mandibular molars. Ph.D. Dissertation, George Washington University.

Skinner, M.M., Gunz, P., Wood, B.A., Hublin, J.-J., 2008. Enamel-dentine junction (EDJ) morphology distinguishes the lower molars of *Australopithecus africanus* and *Paranthropus robustus*. Journal of Human Evolution 55*,* 979-988.

Skinner, M.M., Evans, A., Smith, T., Jernvall, J., Tafforeau, P., Kupczik, K., Olejniczak, A.J., Rosas, A., Radovčić, J., Thackeray, J.F., Toussaint, M., Hublin, J.-J., 2010. Brief communication: Contributions of enamel-dentine junction shape and enamel deposition to primate molar crown complexity. American Journal of Physical Anthropology 142*,* 157-163.

Suwa, G., 1990. A comparative analysis of hominid dental remains from the Shungura and Usno Formations, Omo valley, Ethiopia. Ph.D. Dissertation, University of California, Berkeley.

Suwa, G., Kono, R.T., Simpson, S.W., Asfaw, B., Lovejoy, C.O., White, T.D., 2009. Paleobiological implications of the *Ardipithecus ramidus* dentition. Science 326, 69-99.

Tobias, P.V., 1967. Olduvai Gorge. Vol 2. The Cranium and Maxillary Dentition of *Australopithecus* (*Zinjanthropus*) *boisei*. Cambridge University Press, Cambridge.

Tobias, P.V., 1971. Human skeletal remains from the Cave of Hearths, Makapansgat, northern Transvaal. American Journal of Physical Anthropology 34, 335-367.

Ungar, P.S., Grine, F.E., 1991. Incisor size and wear in *Australopithecus africanus* and *Paranthropus robustus*. Journal of Human Evolution 20*,* 313-340.

Ungar, P.S., Grine, F.E. Teaford, M.F., 2008. Dental microwear and diet of the Plio-Pleistocene hominin *Paranthropus boisei*. PLoS One 3, e2044.

Visualization Sciences Group, 2010. Avizo, Version 6.3. Visualization Sciences Group, Bordeaux.

Walter, R.C., 1994. Age of Lucy and the First Family: single-crystal $^{40}Ar/^{39}Ar$ dating of the Denen Dora and lower Kada Hadar members of the Hadar Formation, Ethiopia. Geology 22, 6-10.

Ward, S.C., Johanson, D.C, Coppens, Y., 1982. Subocclusal morphology and alveolar process relationships of hominid gnathic elements from the Hadar formation: 1974-1977 collections. American Journal of Physical Anthropology 57, 605-630.

Ward, C., Leakey, M., Walker, A., 1999. The new hominid species *Australopithecus anamensis*. Evolutionary Anthropology 7, 197–205.

Ward, C.V., Leakey, M.G., Walker, A., 2001. Morphology of *Australopithecus anamensis* from Kanapoi and Allia Bay, Kenya. Journal of Human Evolution, 41, 255-368.

Ward, C.V., Plavcan, J.M., Manthi, F.K., 2017. New fossils of *Australopithecus anamensis* from Kanapoi, West Turkana, Kenya (2012–2015). Journal of Human Evolution. https://doi.org/10.1016/j.jhevol.2017.07.008

White, T.D., Suwa, G. and Asfaw, B., 1994. *Australopithecus ramidus*, a new species of early hominid from Aramis, Ethiopia. Nature 371, 306-312.

White, T.D., WoldeGabriel, G., Asfaw, B., Ambrose, S., Beyene, Y., Bernor, R.L., Boisserie, J.R., Currie, B., Gilbert, H., Haile-Selassie, Y., Hart, W.K., 2006. Asa Issie, Aramis and the origin of *Australopithecus*. Nature 440, 883-889

Wolfram Research, Inc., 2016. Mathematica, Version 10.4.1. Wolfram Research, Inc., Champaign.

Wollny, G., Kellman, P., Ledesma-Carbayo, M.J., Skinner, M.M., Hublin, J.-J., Hierl, T., 2013. MIA-A free and open source software for gray scale medical image analysis. Source Code for Biology and Medicine 8, 20.

Wood, B.A., 1991. Koobi Fora Research Project: Volume 4. Hominid Cranial Remains. Clarendon Press, Oxford.

Wood, B.A., Aiello, L.C., 1998. Taxonomic and functional implications of mandibular scaling in early hominins. American Journal of Physical Anthropology 105, 523-538

Wood, B., Strait, D., 2004. Patterns of resource use in early *Homo* and *Paranthropus*. Journal of Human Evolution 46*,* 119-162.

Wood, B.A., Uytterschaut, H., 1987. Analysis of the dental morphology of Plio-Pleistocene hominids. III. Mandibular premolar crowns. Journal of Anatomy 154*,* 121-156.

Zanolli, C., Mazurier, A. 2013. Endostructural characterization of the *H. heidelbergensis* dental remains from the early Middle Pleistocene site of Tighenif, Algeria. Comptes Rendus Palevol 12, 293-304.

Zanolli, C., Pan, L., Dumoncel, J., Kullmer, O., Kundrat, M., Liu, W., Macchiarelli, R., Mancini, L., Schrenk, F., Tuniz, C. 2018. Inner tooth morphology of *Homo erectus* from Zhoukoudian. New evidence from an old collection housed at Uppsala University, Sweden. Journal of Human Evolution 116, 1-13.

Figure captions

Figure 1. Landmarking protocol and P_3 terminology guide. A) Example of the landmarking protocol for all three landmark sets. Numbers in brackets indicate the number of landmarks placed in each set, with the EDJ ridge set split into two sections. 1 = protoconid landmark; 2 = metaconid landmark (or homologous point, see text). B) Neanderthal right P_3 in occlusal (top) and distal (bottom) view, illustrating the major morphological features present in the hominoid P_3.

Figure 2. Wireframe images for each well-represented hominoid species included in the sample, showing the mean shape for the EDJ ridge landmark set (blue lines) and CEJ ridge landmark set (black lines), and the mean position of the EDJ main landmarks (blue circles). For each species, the top image shows both landmark sets in lingual view, and the bottom image shows them in occlusal view. For visualization purposes, an example is included for *Homo naledi* in which the wireframe model is overlayed on a surface model of the EDJ. Abbreviations: B = buccal; L = lingual; M = mesial; D = distal.

Figure 3. Results of a PCA of EDJ and CEJ shape, as shown by the first three principal components (PCs). Percentages in brackets indicate the proportion of the total variation in the sample which is explained by each PC. Specimens discussed in the main text are individually labeled, and *Paranthropus robustus* specimens are labeled according to site; Swartkrans (S) or Drimolen (D). Abbreviations: *A.afa = Australopithecus afarensis*; *A.afr = Australopithecus africanus*; *A.ana = Australopithecus anamensis*; *H.nal = Homo naledi*; *H.nea = Homo*

neanderthalensis; H.sap = Extant *Homo sapiens; Pan t.v = Pan troglodytes verus*; *P.boi = Paranthropus boisei*; *P.rob = Paranthropus robustus*.

Figure 4. Results of a PCA of EDJ shape, as shown by the first three principal components (PCs). Percentages in brackets indicate the proportion of the total variation in the sample which is explained by each PC. Abbreviations are the same as in Figure 3.

Figure 5. Boxplot of natural logarithm of centroid size for each taxon. Whiskers represent the highest and lowest data points, boxes represent the first and third quartiles, and the band inside the boxes represents the second quartile (median).

Figure 6. Wireframe models for specimens suggested to represent early *Homo*, with mean wireframe models for *Australopithecus* and late *Homo* for comparison. All are shown in lingual (top) and occlusal (bottom) views. The *Australopithecus* mean model includes specimens of *A. afarensis* and *A. africanus*, whilst the late *Homo* mean model includes specimens of *H. neanderthalensis* and *H. sapiens* (including Qafzeh). Blue lines = EDJ ridge landmarks; black lines = CEJ landmarks; blue circles = main EDJ landmarks. Abbreviations: B = buccal; L = lingual; M = mesial; D = distal

Figure 7. The EDJ and OES in oblique view for a number of hominoid species. Two specimens of *A. afarensis* are included, highlighting the variation in P_3 EDJ morphology seen in this species. The protoconid of AL 266-1 is worn, and was reconstructed here for the

977 purpose of GM analysis. The reconstructed section is shown in blue. Abbreviations: B =

978 buccal; L = lingual; M = mesial; D = distal.

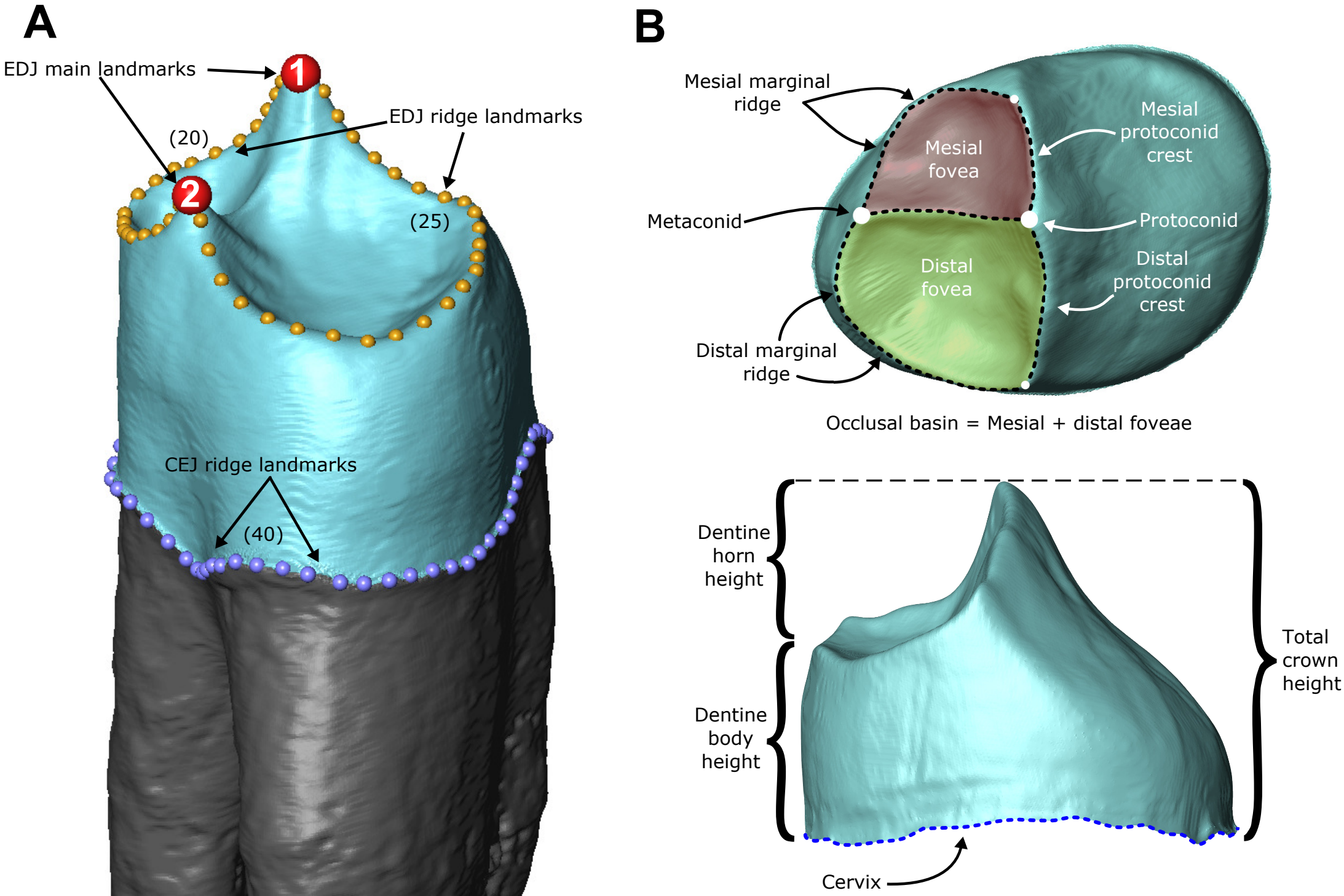
A
EDJ main landmarks
1
2
(20)
EDJ ridge landmarks
(25)
CEJ ridge landmarks
(40)
B
Mesial marginal ridge
Mesial fovea
Mesial protoconid crest
Metaconid
Protoconid
Distal fovea
Distal protoconid crest
Distal marginal ridge
Occlusal basin = Mesial + distal foveae
Dentine horn height
Dentine body height
Total crown height
Cervix

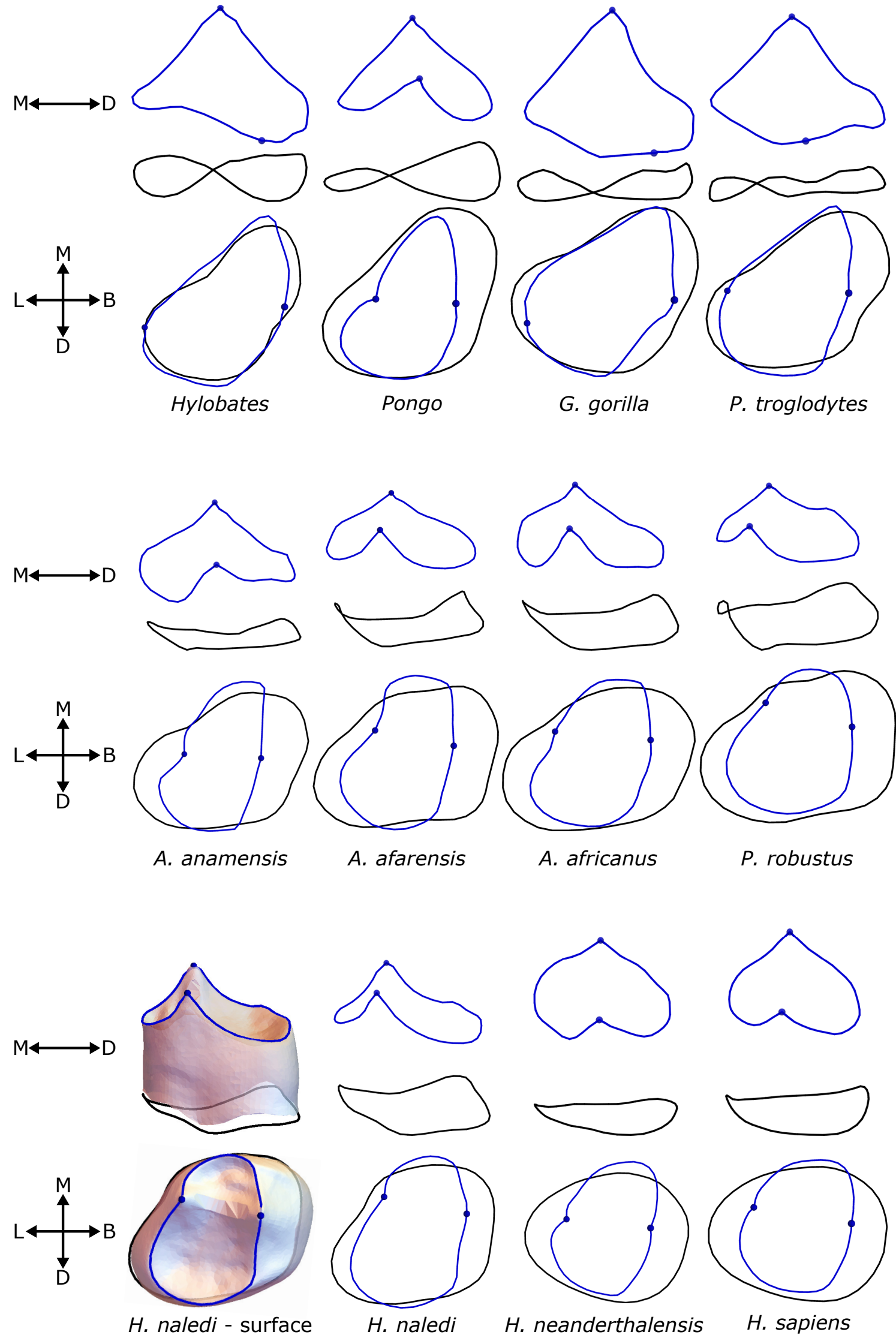
M
D
M
L
B
D
Hylobates
Pongo
G. gorilla
P. troglodytes
M
D
M
L
B
D
A. anamensis
A. afarensis
A. africanus
P. robustus
M
D
M
L
B
D
H. naledi - surface
H. naledi
H. neanderthalensis
H. sapiens

Apes

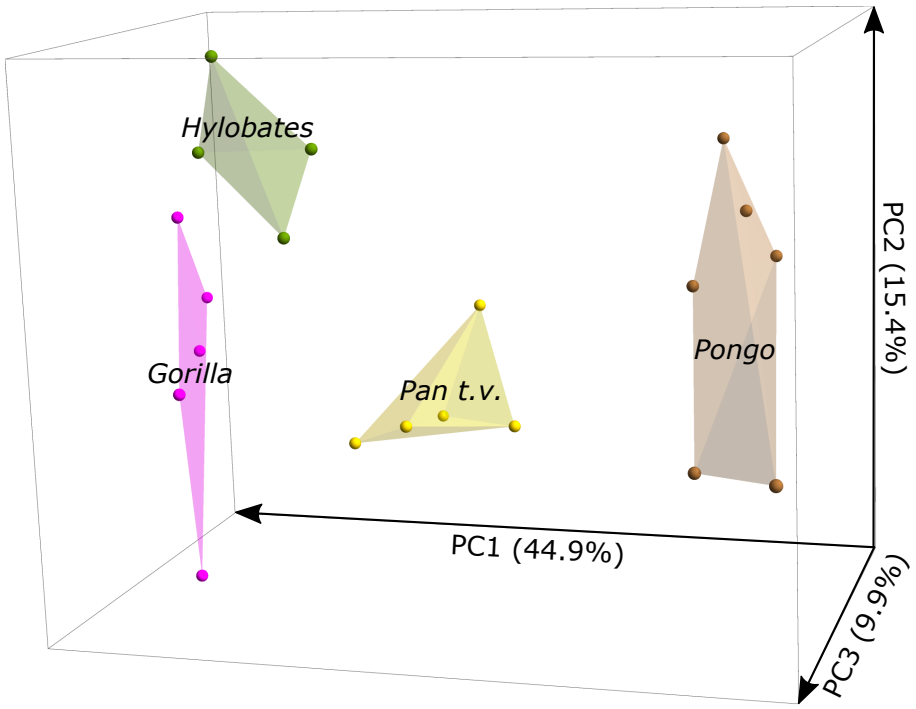

Plio-Pleistocene hominins

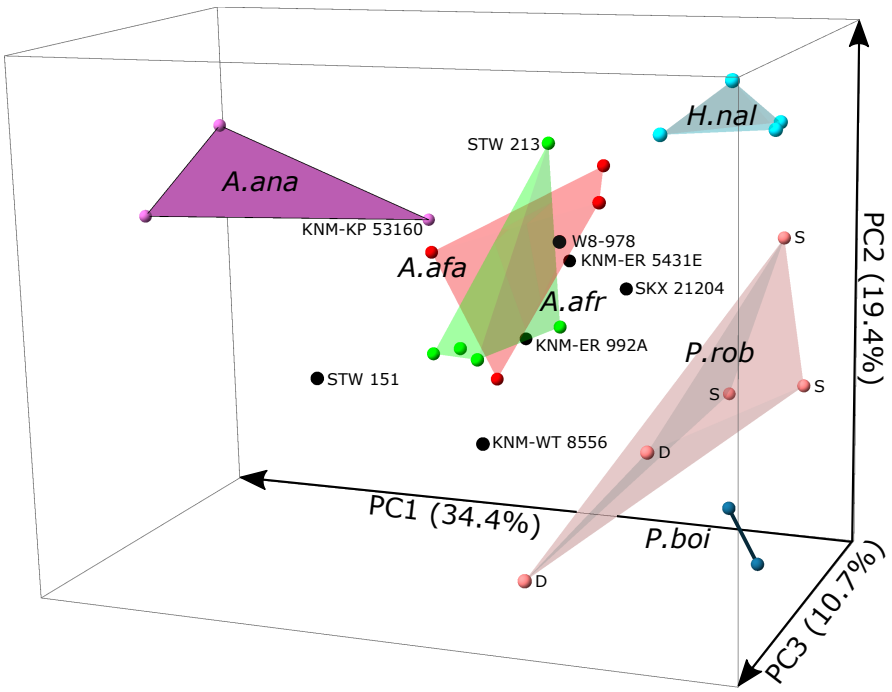

Middle-Late Pleistocene hominins

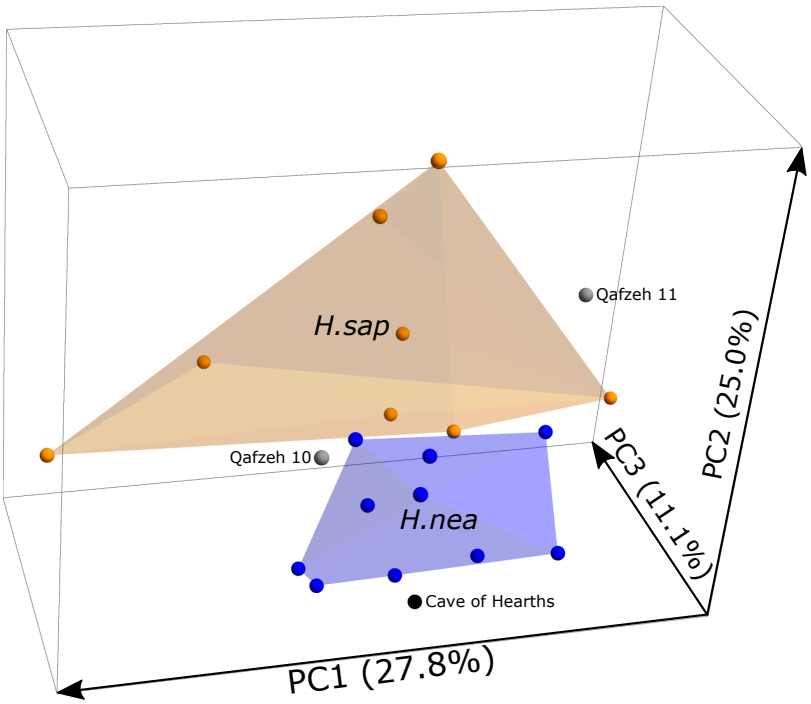

Apes

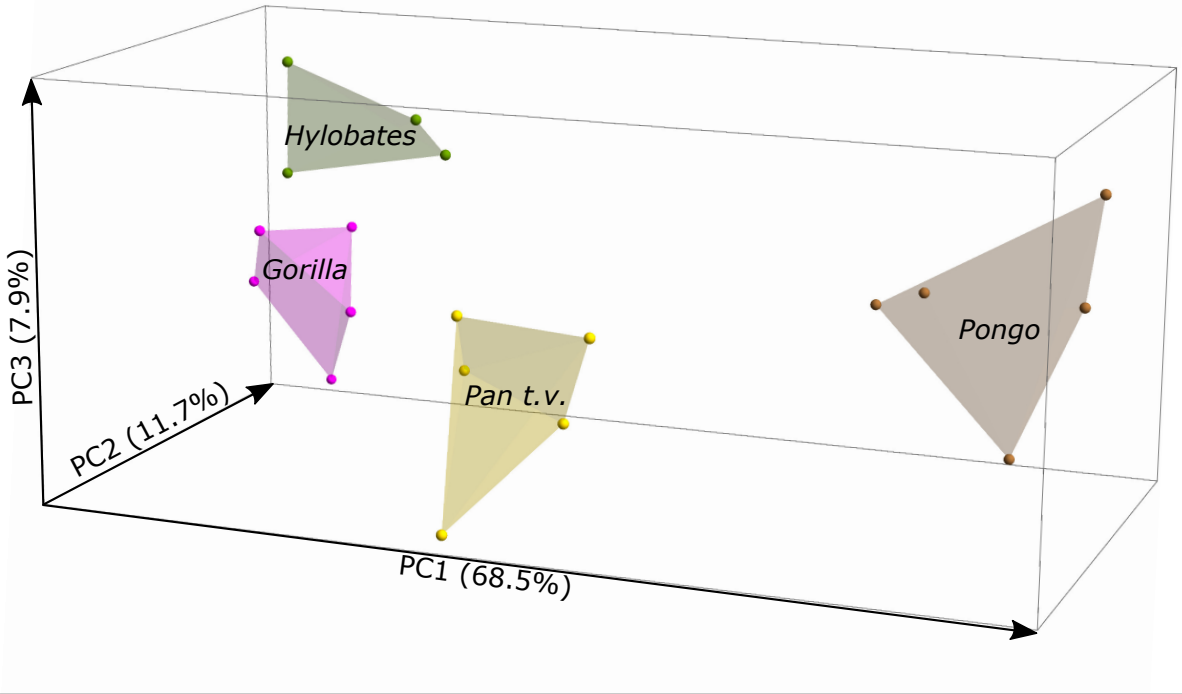

Plio-Pleistocene hominins

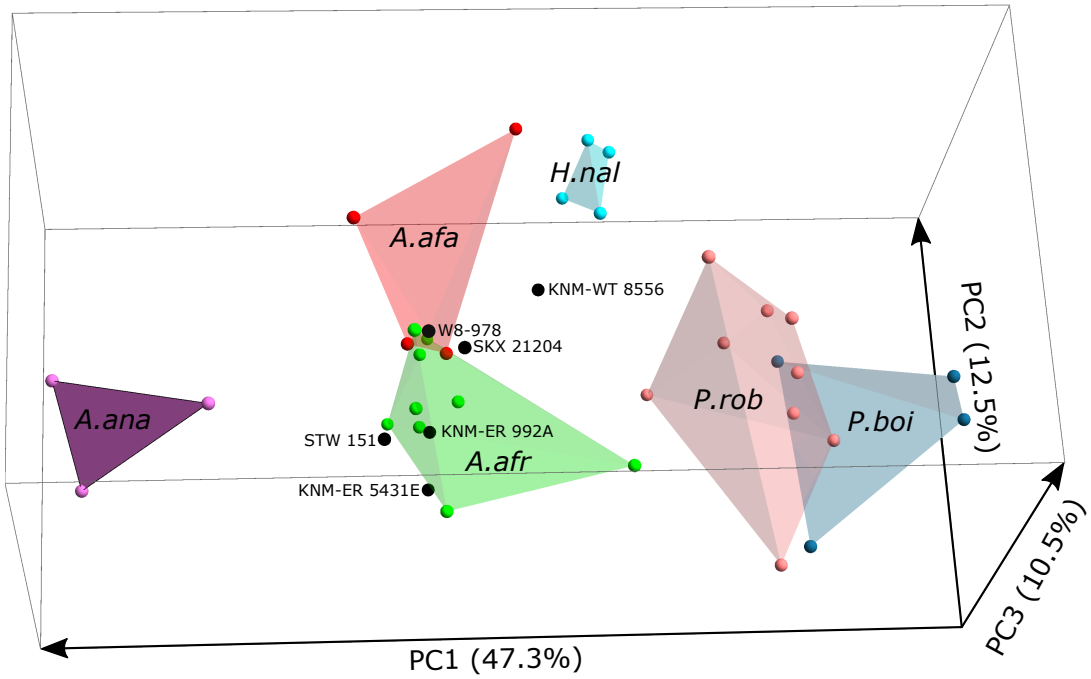

Middle-Late Pleistocene hominins

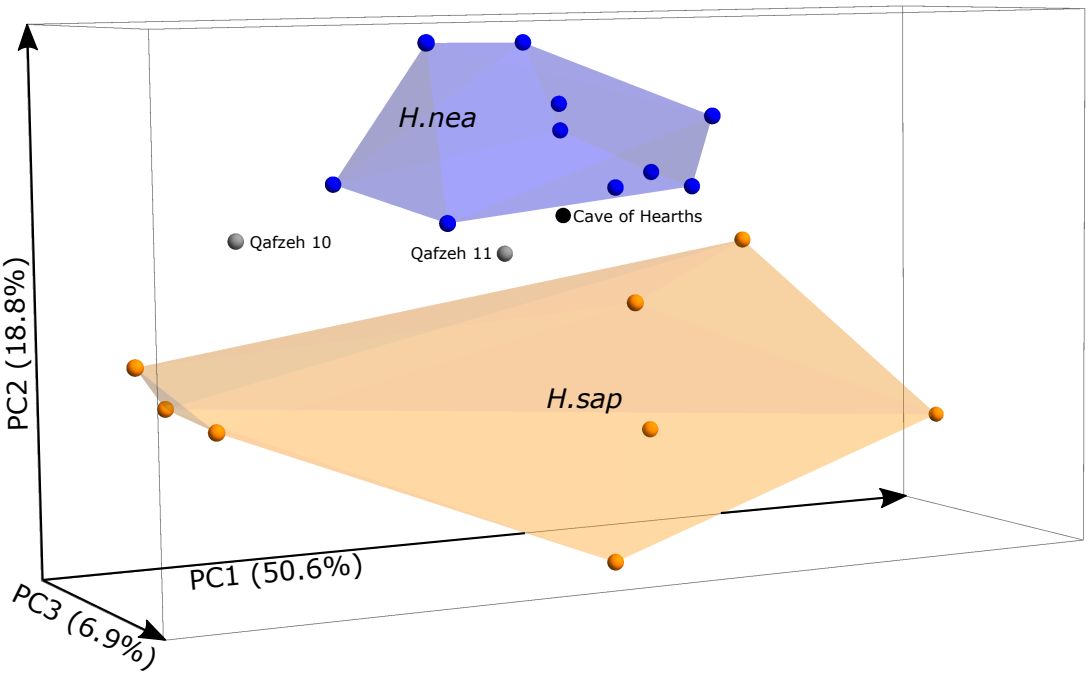

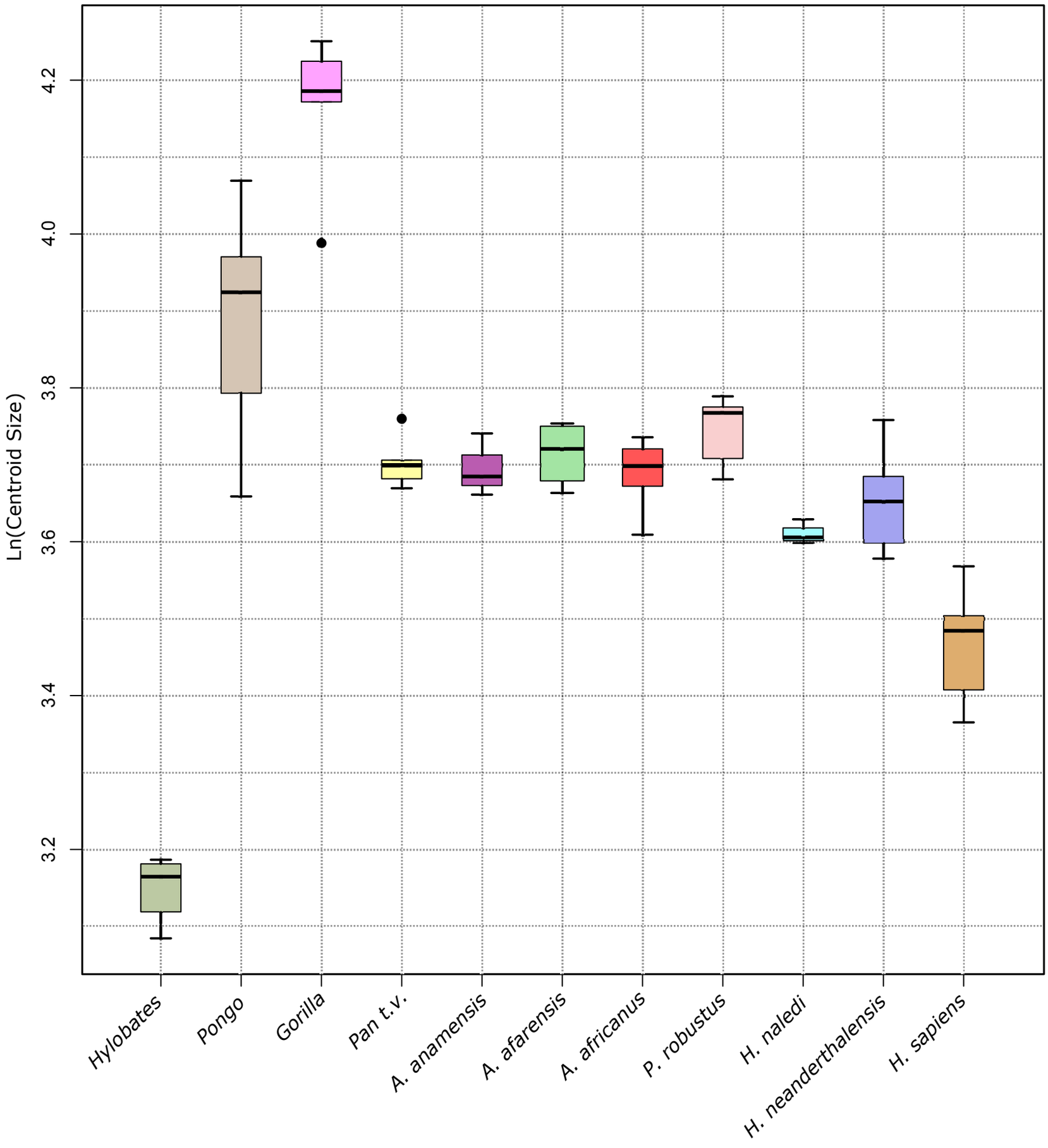
Ln(Centroid Size)
4.2
4.0
3.8
3.6
3.4
3.2
Hylobates
Pongo
Gorilla
Pan t.v.
A. anamensis
A. afarensis
A. africanus
P. robustus
H. naledi
H. neanderthalensis
H. sapiens

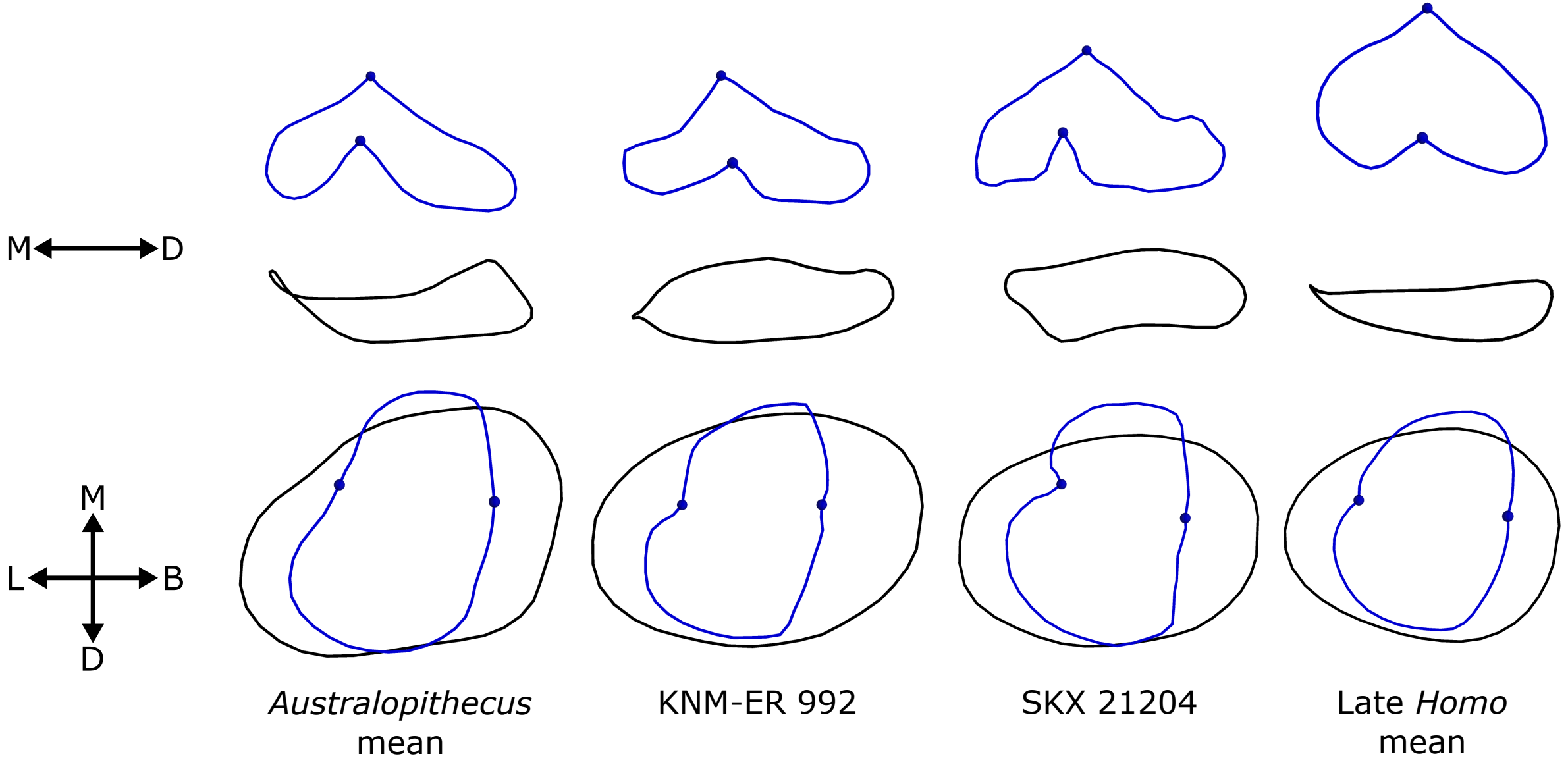
M
D
M
L
B
D
Australopithecus mean
KNM-ER 992
SKX 21204
Late *Homo* mean

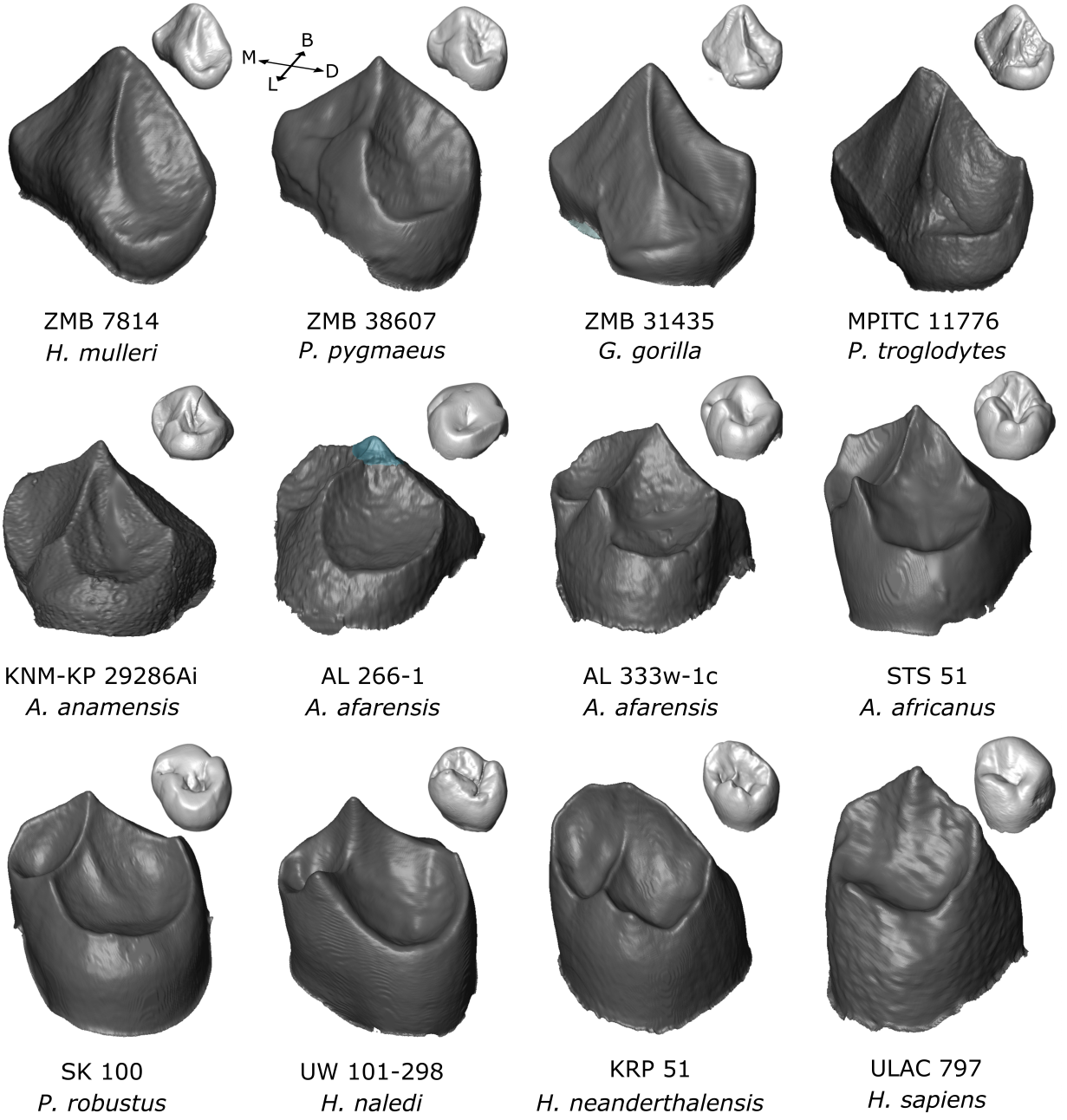
B
M
D
L
ZMB 7814
H. mulleri
ZMB 38607
P. pygmaeus
ZMB 31435
G. gorilla
MPITC 11776
P. troglodytes
KNM-KP 29286Ai
A. anamensis
AL 266-1
A. afarensis
AL 333w-1c
A. afarensis
STS 51
A. africanus
SK 100
P. robustus
UW 101-298
H. naledi
KRP 51
H. neanderthalensis
ULAC 797
H. sapiens

Table 1

Study sample summary. The extant and fossil taxa included in the sample are listed, along with their locality, and the sample size for each of the four different geometric morphometric analyses. Full specimen list can be found in SOM Table S1

Taxon	Locality	CEJ+ EDJ	CEJ+ Med	CEJ only	EDJ only
Hylobates	South East Asia (*Hy. muelleri* and *Hy. agilis*)	4	4	4	4
Pongo	Borneo; Sumatra (*Po. pygmaeus* and *Po. abelii*)	6	6	6	6
Gorilla	Cameroon; Congo (*G. gorilla*)	5	5	5	5
Pan	Côte d'Ivoire (*P. troglodytes verus*)	5	5	5	5
A. anamensis	Kanapoi, Kenya	3	3	3	3
A. afarensis	Hadar, Ethiopia	4	6	9	4
A. africanus	Sterkfontein and Taung, South Africa	5	8	9	9
P. robustus	Drimolen and Swartkrans, South Africa	5	6	8	9
P. boisei	Koobi Fora and West Turkana, Kenya; Omo, Ethiopia	2	2	3	4
Homo sp.	Koobi Fora and West Turkana, Kenya; Swartkrans, South Africa	2	3	7	2
H. naledi	Rising Star cave system, South Africa	4	5	7	4
H. heidelbergensis	Mauer, Germany	0	1	1	0
H. neanderthalensis	Combe Grenal, France; Krapina, Croatia; Scladina, Belgium	10	15	15	10
Fossil *H.* sapiens	Qafzeh, Israel	2	2	2	2
Recent *H. sapiens*	Anatomical collection, various localities	8	12	12	8
Indeterminate[a]	Omo, Ethiopia; West Turkana and Koobi Fora, Kenya; Makapansgat and Sterkfontein, South Africa	5	5	5	5

Abbreviations: CEJ = cementum-enamel junction; EDJ = enamel-dentine junction; Med = Metaconid.

[a] Indeterminate specimens are W8-978, KNM-WT 8556, KNM-ER 5431E, the Cave of Hearths mandible and STW 151.

Table 2

Pairwise comparisons of P_3 centroid size.[a]

	Hy	*Pongo*	*Gor*	*Pan*	*A. ana*	*A. afa*	*A. afri*	*P. rob*	*H. nal*	*H. nea*
Pongo	**0.019**	—	—	—	—	—	—	—	—	—
Gor	**0.019**	**0.019**	—	—	—	—	—	—	—	—
Pan	**0.019**	**0.049**	**0.019**	—	—	—	—	—	—	—
A. ana	**0.046**	0.108	**0.033**	0.796	—	—	—	—	—	—
A. afa	**0.046**	0.093	**0.031**	0.709	0.585	—	—	—	—	—
A. afri	**0.019**	**0.046**	**0.019**	0.618	0.839	0.473	—	—	—	—
P. rob	**0.019**	0.085	**0.019**	0.158	0.239	0.404	0.124	—	—	—
H. nal	**0.046**	**0.020**	**0.019**	**0.019**	**0.046**	**0.046**	**0.049**	**0.031**	—	—
H. nea	**0.007**	**0.006**	**0.006**	0.108	0.290	0.101	0.274	**0.019**	0.248	—
H. sap	**0.010**	**0.006**	**0.006**	**0.006**	**0.019**	**0.010**	**0.006**	**0.006**	**0.019**	**0.002**

Abbreviations: *A. afa* = *A. afarensis*; *A. afri* = *Australopithecus africanus*; *A. ana* = *Australopithecus anamensis*; *H. nal* = *Homo naledi*; *H. nea* = *Homo neanderthalensis*; *H. sap* = *Homo sapiens Hy* = *Hylobates*; *Gor* = *Gorilla gorilla; Pan* = *Pan troglodytes verus*; *P. rob* = *Paranthropus robustus.*

[a] Bold indicates $p < 0.05$ (*p*-values were calculated using a permutation test with 100,000 repeats).

Table 3

Pairwise comparisons of P_3 mean Procrustes shape.[a]

	Hy	*Pongo*	*Gor*	*Pan*	*A. ana*	*A. afa*	*A. afri*	*P. rob*	*H. nal*	*H. nea*
Pongo	**0.029**	—	—	—	—	—	—	—	—	—
Gor	0.125	**0.029**	—	—	—	—	—	—	—	—
Pan	0.117	**0.029**	0.135	—	—	—	—	—	—	—
A. ana	0.156	**0.035**	**0.035**	0.067	—	—	—	—	—	—
A. afa	**0.044**	**0.035**	**0.046**	0.063	0.133	—	—	—	—	—
A. afri	0.063	**0.035**	**0.029**	**0.029**	0.171	0.754	—	—	—	—
P. rob	0.063	**0.035**	**0.029**	**0.029**	0.112	0.462	0.170	—	—	—
H. nal	**0.044**	**0.035**	**0.029**	**0.035**	**0.044**	**0.044**	**0.046**	0.143	—	—
H. nea	**0.035**	**0.029**	**0.023**	**0.035**	**0.029**	**0.023**	**0.029**	**0.029**	**0.023**	—
H. sap	**0.029**	**0.035**	**0.029**	0.054	**0.035**	**0.041**	**0.035**	**0.035**	**0.035**	0.236

Abbreviations: *A. afa* = *A. afarensis*; *A. afri* = *Australopithecus africanus*; *A. ana* = *Australopithecus anamensis*; *H. nal* = *Homo naledi*; *H. nea* = *Homo neanderthalensis*; *H. sap* = *Homo sapiens Hy* = *Hylobates*; *Gor* = *Gorilla gorilla; Pan* = *Pan troglodytes verus*; *P. rob* = *Paranthropus robustus.*

[a] Bold indicates $p < 0.05$ (p-values were calculated using a permutation test with 100,000 repeats).

Table 4

The hominoid P_3 classification accuracies per analysis.

Analysis	PCs used	Accuracy (%)
EDJ+CEJ	7	88
EDJ only	5	87
CEJ only	4	69
CEJ+Med	5	80

Abbreviations: CEJ = cementum-enamel junction; EDJ = enamel-dentine junction; Med = Metaconid; PCs = principal components.

Supplementary Online Material (SOM):

Endostructural morphology in hominoid mandibular third premolars: Geometric morphometric analysis of dentine crown shape

Thomas W. Davies[a,b,*], Lucas K. Delezene[c], Philipp Gunz[b], Jean-Jacques Hublin[b], Matthew M. Skinner[a,b]

[a] *School of Anthropology and Conservation, University of Kent, Canterbury, CT2 7NZ, UK*
[b] *Department of Human Evolution, Max Planck Institute for Evolutionary Anthropology, Deutscher Platz 6, 04103 Leipzig, Germany*
[c]*Department of Anthropology, University of Arkansas, Fayetteville, Arkansas, 72701 USA*

*Corresponding author.
E-mail address: thomas_davies@eva.mpg.de (T.W. Davies).

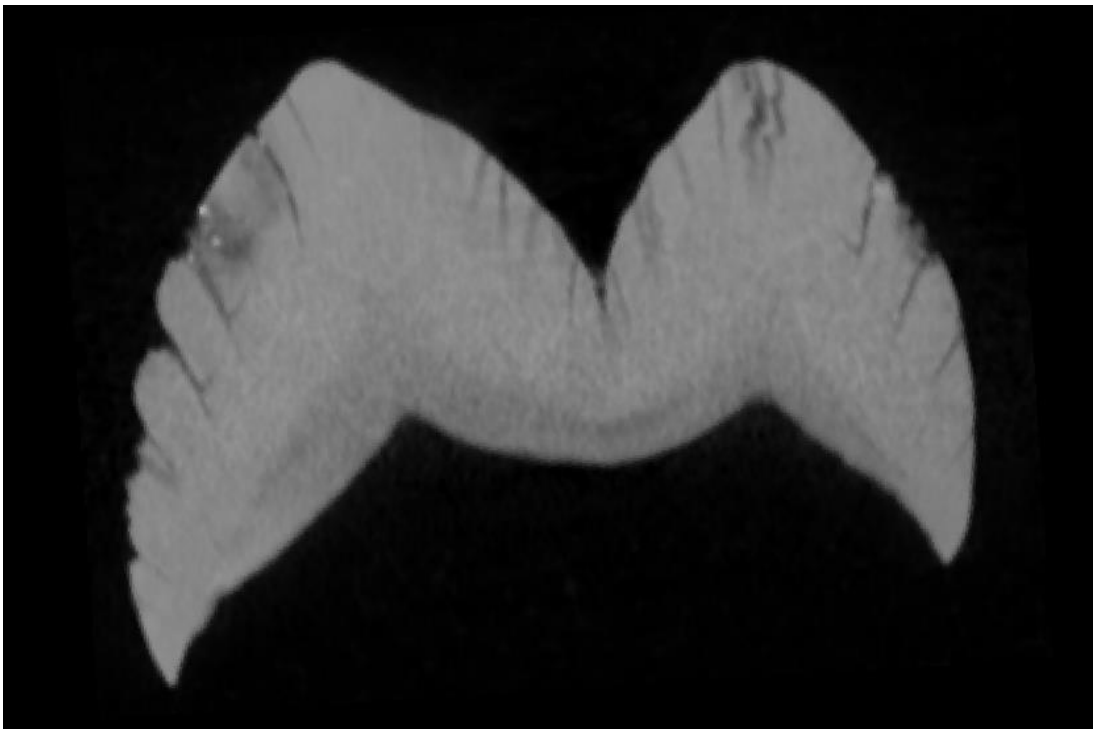

SOM Figure S1. Example slice from a CT scan with very low tissue distinction—grayscale values for enamel and dentine are mostly indistinguishable in this case, preventing segmentation of the enamel-dentine junction. The specimen shown is KNM-ER 1477D (*Paranthropus boisei*).

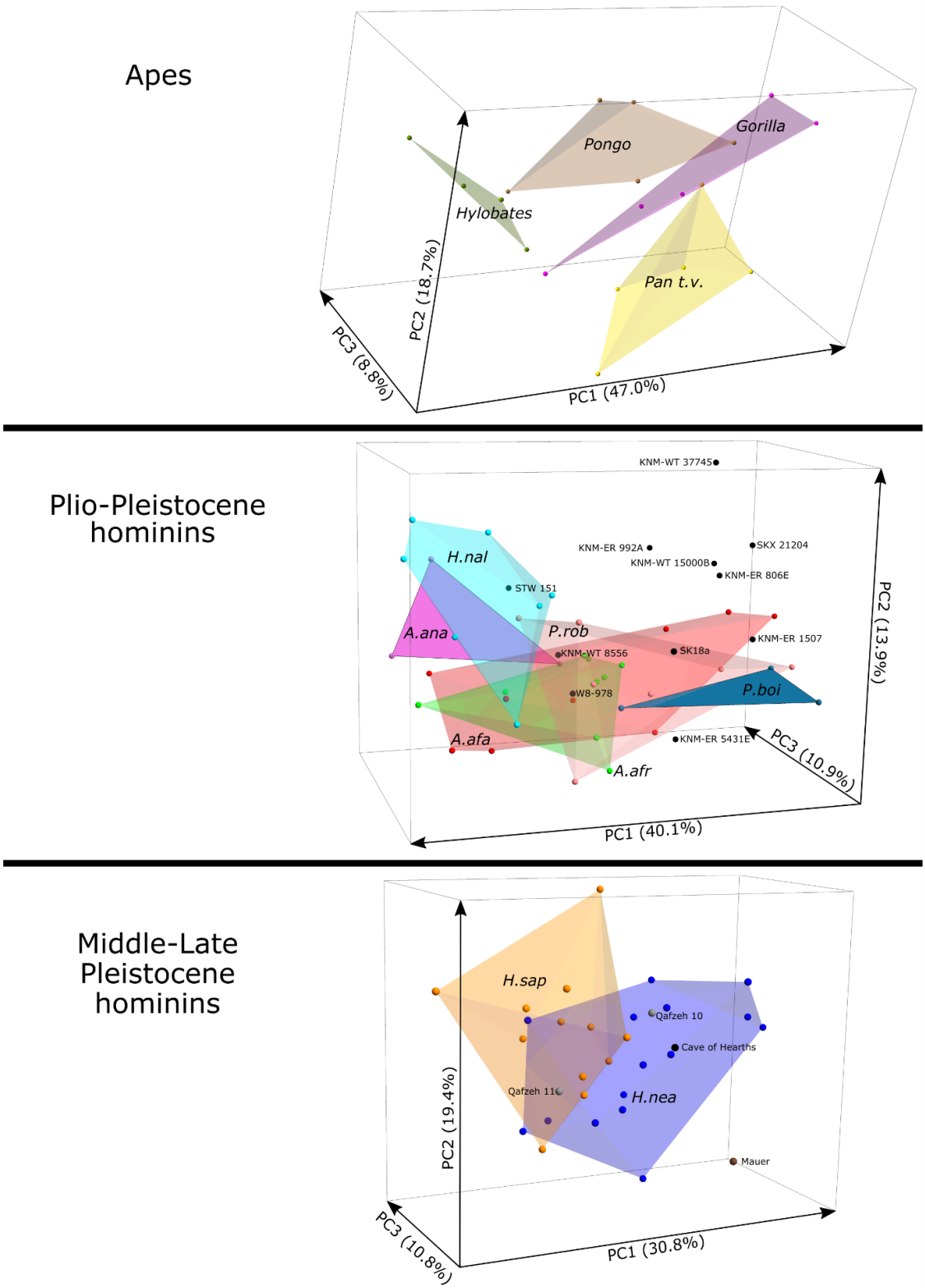

SOM Figure S2. Results of a principal components analysis (PCA) of cementum-enamel junction shape, as shown by a plot of the first three principal components (PCs). Percentages in brackets indicate the proportion of the total variation in the sample which is explained by each PC. Abbreviations: *A.afa* = *Australopithecus afarensis*; *A.afr* = *Australopithecus africanus*; *A.ana* = *Australopithecus anamensis*; *H.nal* = *Homo naledi*; *H.nea* = *Homo neanderthalensis*; *H.sap* = extant *Homo sapiens; Pan t.v* = *Pan troglodytes verus*; *P.boi* = *Paranthropus boisei*; *P.rob* = *Paranthropus robustus*.

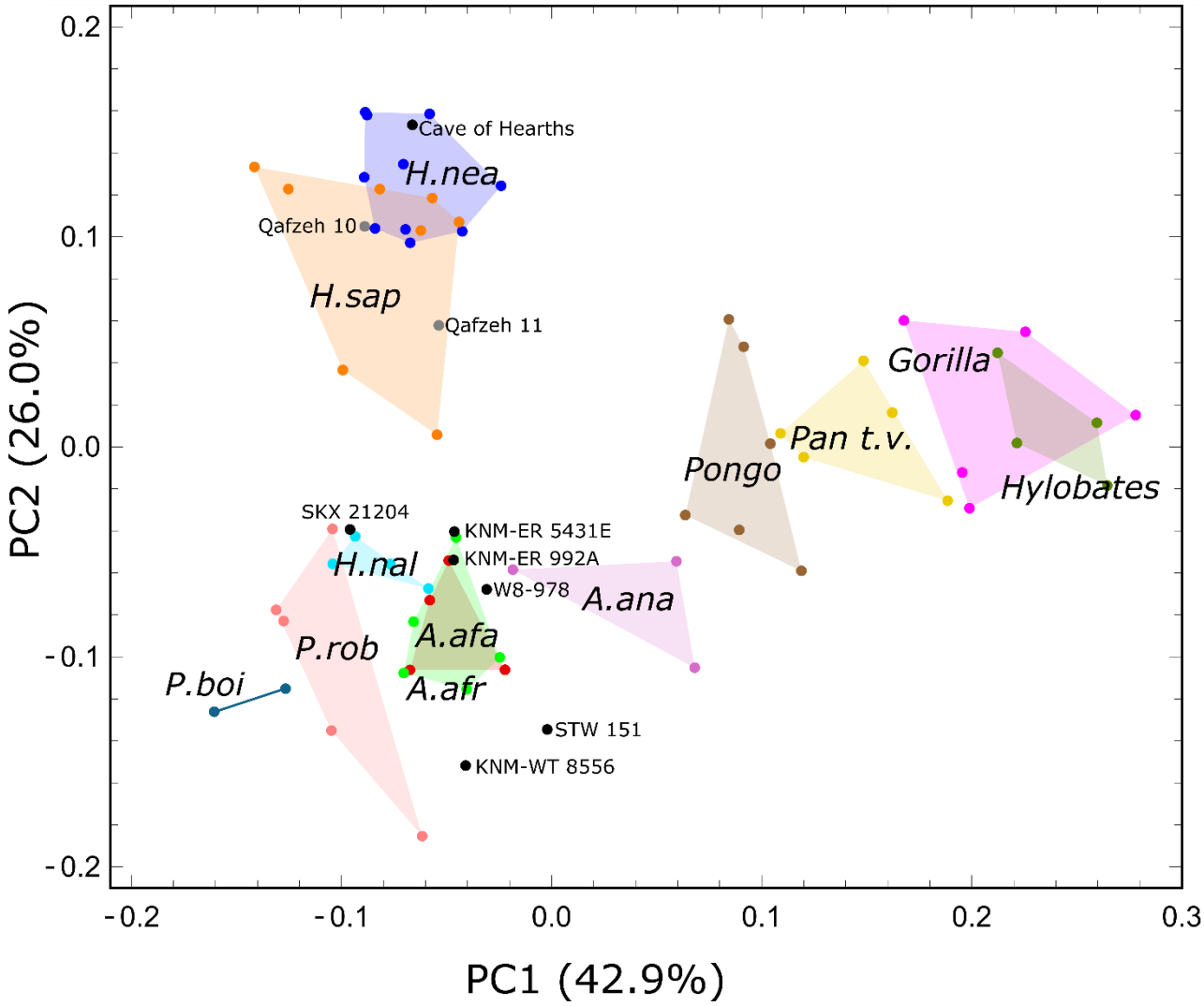

SOM Figure 3. Results of a principal components analysis (PCA) of EDJ + CEJ shape for all specimens, as shown by a plot of the first two principal components (PC). Percentages in brackets indicate the proportion of the total variation in the sample which is explained by each PC. Abbreviations: *A.afa* = *Australopithecus afarensis*; *A.afr* = *Australopithecus africanus*; *A.ana* = *Australopithecus anamensis*; *H.nal* = *Homo naledi*; *H.nea* = *Homo neanderthalensis*; *H.sap* = Extant *Homo sapiens; Pan t.v* = *Pan troglodytes verus*; *P.boi* = *Paranthropus boisei*; *P.rob* = *Paranthropus robustus*.

SOM Table S1

Detailed study sample, including which analyses each specimen is included in.

Specimen	Side	Site/Origin	Taxon	Source	Position basis[a]	Position source	EDJ+ CEJ	CEJ + Med	CEJ only	EDJ only	ln(CS)	Recon ?
ZMB 7814	L	Borneo	*Hylobates muelleri*	ZMB records	1	ZMB records	Y	Y	Y	Y	3.0847	—
ZMB 7826	L	Borneo	*Hylobates muelleri*	ZMB records	1	ZMB records	Y	Y	Y	Y	3.1760	—
ZMB 7828	L	Borneo	*Hylobates muelleri*	ZMB records	1	ZMB records	Y	Y	Y	Y	3.1536	—
ZMB 85368	L	Sumatra, Indonesia	*Hylobates agilis*	ZMB records	1	ZMB records	Y	Y	Y	Y	3.1867	Prd
ZMB 6948	R	Borneo	*Pongo pygmaeus*	ZMB records	1	ZMB records	Y	Y	Y	Y	3.9207	Prd
ZMB 6957	L	Borneo	*Pongo pygmaeus*	ZMB records	1	ZMB records	Y	Y	Y	Y	3.7932	—
ZMB 12209	R	Sumatra, Indonesia	*Pongo abelii*	ZMB records	1	ZMB records	Y	Y	Y	Y	3.9706	Prd
ZMB 38607	R	Sumatra, Indonesia	*Pongo abelii*	ZMB records	1	ZMB records	Y	Y	Y	Y	3.6590	—
ZMB 83509	R	Sumatra, Indonesia	*Pongo abelii*	ZMB records	1	ZMB records	Y	Y	Y	Y	3.9283	—
ZMB 83511	L	Sumatra, Indonesia	*Pongo abelii*	ZMB records	1	ZMB records	Y	Y	Y	Y	4.0695	Prd
ZMB 17963	L	Cameroon	*Gorilla gorilla*	ZMB records	1	ZMB records	Y	Y	Y	Y	4.2510	Prd
ZMB 30940	R	Cameroon	*Gorilla gorilla*	ZMB records	1	ZMB records	Y	Y	Y	Y	4.2249	—
ZMB 30941	L	Congo	*Gorilla gorilla*	ZMB records	1	ZMB records	Y	Y	Y	Y	4.1720	Prd
ZMB 31435	R	Cameroon	*Gorilla gorilla*	ZMB records	1	ZMB records	Y	Y	Y	Y	3.9884	—
ZMB 83561	R	Cameroon	*Gorilla gorilla*	ZMB records	1	ZMB records	Y	Y	Y	Y	4.1861	Prd
MPITC 11776	L	Taï, Côte d'Ivoire	*Pan troglodytes verus*	MPI records	1	MPI records	Y	Y	Y	Y	3.6820	—
MPITC 11800	R	Taï, Côte d'Ivoire	*Pan troglodytes verus*	MPI records	1	MPI records	Y	Y	Y	Y	3.6696	—
MPITC 11903	R	Taï, Côte d'Ivoire	*Pan troglodytes verus*	MPI records	1	MPI records	Y	Y	Y	Y	3.6994	Prd
MPITC 13430	R	Taï, Côte d'Ivoire	*Pan troglodytes verus*	MPI records	1	MPI records	Y	Y	Y	Y	3.7598	—
MPITC 13437	R	Taï, Côte d'Ivoire	*Pan troglodytes verus*	MPI records	1	MPI records	Y	Y	Y	Y	3.7061	—
KNM-KP 29281	R	Kanapoi, Kenya	*Australopithecus anamensis*	Leakey et al., 1995	1	Ward et al., 2001	Y	Y	Y	Y	3.6614	—
KNM-KP 29286	R	Kanapoi, Kenya	*Australopithecus anamensis*	Leakey et al. 1995	1	Ward et al., 2001	Y	Y	Y	Y	3.7409	—
KNM-KP 53160	L	Kanapoi, Kenya	*Australopithecus anamensis*	Ward et al. 2017	1	Ward et al. 2017	Y	Y	Y	Y	3.6851	—
AL128-23	R	Hadar, Ethiopia	*Australopithecus afarensis*	Johanson et al., 1982	1	Johanson et al., 1982	N	Y	Y	N	—	—
AL266-1	R	Hadar, Ethiopia	*Australopithecus afarensis*	Johanson et al., 1982	1	Johanson et al., 1982	Y	Y	Y	Y	3.6636	Prd
AL277-1	L	Hadar, Ethiopia	*Australopithecus afarensis*	Johanson et al., 1982	1	Johanson et al., 1982	N	N	Y	N	—	—
AL333-10	L	Hadar, Ethiopia	*Australopithecus afarensis*	Johanson et al., 1982	3	Johanson et al., 1982	Y	Y	Y	Y	3.7539	Prd
AL333w-1c	R	Hadar, Ethiopia	*Australopithecus afarensis*	Johanson et al., 1982	2	Johanson et al., 1982	Y	Y	Y	Y	3.7468	—

AL400-1a	R	Hadar, Ethiopia	*Australopithecus afarensis*	Johanson et al., 1982	1	Johanson et al., 1982	N	N	Y	N	—	—
AL417-1a	L	Hadar, Ethiopia	*Australopithecus afarensis*	Kimbel et al., 1994	1	Kimbel et al., 1994	N	Y	Y	N	—	—
AL655-1	L	Hadar, Ethiopia	*Australopithecus afarensis*	Kimbel and Delezene, 2009	3	Kimbel and Delezene, 2009	Y	Y	Y	Y	3.6950	—
AL1045	R	Hadar, Ethiopia	*Australopithecus afarensis*	Kimbel and Delezene, 2009	1	Kimbel and Delezene, 2009	N	N	Y	N	—	—
W8-978	R	Omo, Ethiopia	Indet.	Suwa, 1990	3	Suwa, 1990	Y	Y	Y	Y	3.6459	—
KNM-WT 8556	L	West Turkana, Kenya	Indet.	Brown et al., 2001	1	Brown et al., 2001	Y	Y	Y	Y	3.7714	—
STW 7	L	Sterkfontein, South Africa	*Australopithecus africanus*	Moggi-Cecchi et al., 2006	3	Moggi-Cecchi et al., 2006	Y	Y	Y	Y	3.7210	Prd
STW 104	L	Sterkfontein, South Africa	*Australopithecus africanus*	Moggi-Cecchi et al., 2006	1	Moggi-Cecchi et al., 2006	N	N	N	Y	—	—
STW 142	R	Sterkfontein, South Africa	*Australopithecus africanus*	Moggi-Cecchi et al., 2006	1	Moggi-Cecchi et al., 2006	N	Y	Y	N	—	Med
STW 193	R	Sterkfontein, South Africa	*Australopithecus africanus*	Moggi-Cecchi et al., 2006	2	Moggi-Cecchi et al., 2006	N	N	Y	N	—	—
STW 213	R	Sterkfontein, South Africa	*Australopithecus africanus*	Moggi-Cecchi et al., 2006	2	Moggi-Cecchi et al., 2006	Y	Y	Y	Y	3.6093	Prd
STW 401	R	Sterkfontein, South Africa	*Australopithecus africanus*	Moggi-Cecchi et al., 2006	3	Moggi-Cecchi et al., 2006	N	Y	Y	N	—	Med
STW 404	R	Sterkfontein, South Africa	*Australopithecus africanus*	Moggi-Cecchi et al., 2006	1	Moggi-Cecchi et al., 2006	Y	Y	Y	Y	3.6723	Prd
STW 420B	L	Sterkfontein, South Africa	*Australopithecus africanus*	Moggi-Cecchi et al., 2006	2	Moggi-Cecchi et al., 2006	N	N	N	Y	—	—
STW 498c	L	Sterkfontein, South Africa	*Australopithecus africanus*	Moggi-Cecchi et al., 2006	1	Moggi-Cecchi et al., 2006	N	Y	Y	N	—	—
STS 24	L	Sterkfontein, South Africa	*Australopithecus africanus*	Brain, 1981	1	Brain, 1981	N	N	N	Y	—	—
STS 51	R	Sterkfontein, South Africa	*Australopithecus africanus*	Brain, 1981	2	Brain, 1981	Y	Y	Y	Y	3.6985	—
STS 52b	R	Sterkfontein, South Africa	*Australopithecus africanus*	Dart, 1954	1	Dart, 1954	Y	Y	Y	Y	3.7360	Prd
Taung1	R	Taung, South Africa	*Australopithecus africanus*	Dart, 1925	1	Dart, 1925	N	N	N	Y	—	—
DNH8	L	Drimolen, South Africa	*Paranthropus robustus*	Moggi-Cecchi et al., 2010	1	Moggi-Cecchi et al., 2010	Y	Y	Y	Y	3.7677	—

DNH46	R	Drimolen, South Africa	*Paranthropus robustus*	Moggi-Cecchi et al., 2010	1	Moggi-Cecchi et al., 2010	Y	Y	Y	Y	3.6812	—
DNH51	R	Drimolen, South Africa	*Paranthropus robustus*	Moggi-Cecchi et al., 2010	1	Moggi-Cecchi et al., 2010	N	N	Y	N	—	—
DNH107	L	Drimolen, South Africa	*Paranthropus robustus*	Museum records	2	Museum records	N	N	N	Y	—	—
SK23	L	Swartkrans, South Africa	*Paranthropus robustus*	Robinson, 1956	1	Robinson, 1956	N	Y	Y	N	—	—
SK30	L	Swartkrans, South Africa	*Paranthropus robustus*	Robinson, 1956	3	Robinson, 1956	N	N	Y	N	—	—
SK61	R	Swartkrans, South Africa	*Paranthropus robustus*	Robinson, 1956	1	Robinson, 1956	N	N	N	Y	—	—
SK62	L	Swartkrans, South Africa	*Paranthropus robustus*	Robinson, 1956	1	Robinson, 1956	N	N	N	Y	—	—
SK63	L	Swartkrans, South Africa	*Paranthropus robustus*	Robinson, 1956	1	Robinson, 1956	N	N	N	Y	—	—
SK100	R	Swartkrans, South Africa	*Paranthropus robustus*	Robinson, 1956	3	Oakley, 1977	Y	Y	Y	Y	3.7753	—
SK857	R	Swartkrans, South Africa	*Paranthropus robustus*	Robinson, 1956	3	Oakley, 1977	Y	Y	Y	Y	3.7891	—
SKW5	R	Swartkrans, South Africa	*Paranthropus robustus*	Grine and Daegling, 1993	1	Grine and Daegling, 1993	Y	Y	Y	Y	3.7084	Prd
KNM-ER 1820	L	Koobi Fora, Kenya	*Paranthropus boisei*	Wood, 1991	1	Wood, 1991	N	N	N	Y	—	—
KNM-ER 6082	L	Koobi Fora, Kenya	*Paranthropus boisei*	Wood, 1991	3	Wood, 1991	N	N	N	Y	—	—
KNM-ER 15951H	L	Koobi Fora, Kenya	*Paranthropus boisei*	Wood and Leakey, 2011	2	Wood and Leakey, 2011	N	N	Y	N	—	—
KNM-WT 16005	L	West Turkana, Kenya	*Paranthropus boisei*	Leakey and Walker, 1988	1	Leakey and Walker, 1988	Y	Y	Y	Y	3.9109	Prd
L427-7	R	Omo, Ethiopia	*Paranthropus boisei*	Suwa et al., 1996	1	Suwa et al., 1996	Y	Y	Y	Y	3.7854	—
KNM-ER 806E	L	Koobi Fora, Kenya	*Homo* sp. (*Homo ergaster*)	Wood, 1991	2	Wood, 1991	N	Y	Y	N	—	—
KNM-ER 992A	R	Koobi Fora, Kenya	*Homo* sp. (*Homo ergaster*)	Wood, 1991	1	Wood, 1991	Y	Y	Y	Y	3.7503	Prd
KNM-ER 1507	L	Koobi Fora, Kenya	*Homo* sp.	Leakey and Wood, 1974	1	Leakey and Wood, 1974	N	N	Y	N	—	—
KNM-ER 5431E	L	Koobi Fora, Kenya	Indet.	Wood, 1991	2	Wood, 1991	Y	Y	Y	Y	3.7965	—
KNM-WT 15000B	R	West Turkana, Kenya	*Homo* sp. (*Homo ergaster*)	Walker and Leakey, 1993	1	Walker and Leakey, 1993	N	N	Y	N	—	—
KNM-WT 37745	R	West Turkana, Kenya	*Homo* sp. (*Homo ergaster*)	Prat et al., 2003	3	Prat et al., 2003	N	N	Y	N	—	—
SK 18a	L	Swartkrans, South Africa	*Homo* sp.	Broom and Robinson, 1952		Broom and Robinson, 1952	N	N	Y	N	—	—
SKX 21204	R	Swartkrans, South Africa	*Homo* sp.	Grine, 1989	1	Grine, 1989	Y	Y	Y	Y	3.5498	—
STW 151	R	Sterkfontein, South Africa	Indet.	Moggi-Cecchi et al., 1998	1	Moggi-Cecchi et al., 1998	Y	Y	Y	Y	3.6985	—

U.W. 101-0010	R	Rising Star, South Africa	*Homo naledi*	Berger et al., 2015	1	Berger et al., 2015	N	Y	Y	N	—	—
U.W. 101-0144	L	Rising Star, South Africa	*Homo naledi*	Berger et al., 2015	3	Berger et al., 2015	Y	Y	Y	Y	3.5987	—
U.W. 101-0850	R	Rising Star, South Africa	*Homo naledi*	Berger et al., 2015	3	Berger et al., 2015	N	N	Y	N	—	—
U.W. 101-0889	L	Rising Star, South Africa	*Homo naledi*	Berger et al., 2015	3	Berger et al., 2015	Y	Y	Y	Y	3.6044	—
U.W. 101-1261	R	Rising Star, South Africa	*Homo naledi*	Berger et al., 2015	1	Berger et al., 2015	Y	Y	Y	Y	3.6070	Prd
U.W. 101-1565	L	Rising Star, South Africa	*Homo naledi*	Berger et al., 2015	1	Berger et al., 2015	Y	Y	Y	Y	3.6293	—
U.W. 102-0023	R	Rising Star, South Africa	*Homo naledi*	Hawks et al., 2017	3	Hawks et al., 2017	N	N	Y	N	—	—
Cave of hearths	R	Cave of hearths, South Africa	Indet.	Tobias, 1971	1	Tobias, 1971	Y	Y	Y	Y	3.5517	—
Mauer 1	R	Mauer, Germany	*Homo heidelbergensis*	Schoetensack, 1908	1	Schoetensack, 1908	N	Y	Y	N	—	—
Combe-Grenal I	R	Combe Grenal, France	*Homo neanderthalensis*	Garralda and Vandermeersch, 2000	1	Garralda and Vandermeersch, 2000	Y	Y	Y	Y	3.7012	—
Combe-Grenal XV	R	Combe Grenal, France	*Homo neanderthalensis*	Garralda and Vandermeersch, 2000	3	Garralda and Vandermeersch, 2000	N	Y	Y	N	—	—
KRP 51	R	Krapina, Croatia	*Homo neanderthalensis*	Radovčić, 1988	1	Radovčić, 1988	Y	Y	Y	Y	3.5985	—
KRP 52	L	Krapina, Croatia	*Homo neanderthalensis*	Radovčić, 1988	1	Radovčić, 1988	Y	Y	Y	Y	3.6027	—
KRP 54	L	Krapina, Croatia	*Homo neanderthalensis*	Radovčić, 1988	1	Radovčić, 1988	Y	Y	Y	Y	3.5783	—
KRP 55	L	Krapina, Croatia	*Homo neanderthalensis*	Radovčić, 1988	1	Radovčić, 1988	Y	Y	Y	Y	3.6381	—
KRP 58	R	Krapina, Croatia	*Homo neanderthalensis*	Radovčić, 1988	1	Radovčić, 1988	N	Y	Y	N	-	—
KRP D27	L	Krapina, Croatia	*Homo neanderthalensis*	Radovčić, 1988	2	Radovčić, 1988	N	Y	Y	N	-	—
KRP D28	R	Krapina, Croatia	*Homo neanderthalensis*	Radovčić, 1988	2	Radovčić, 1988	N	Y	Y	N	-	—
KRP D29	R	Krapina, Croatia	*Homo neanderthalensis*	Radovčić, 1988	2	Radovčić, 1988	N	Y	Y	N	-	—
KRP D33	L	Krapina, Croatia	*Homo neanderthalensis*	Radovčić, 1988	2	Radovčić, 1988	Y	Y	Y	Y	3.6851	—
KRP D34	R	Krapina, Croatia	*Homo neanderthalensis*	Radovčić, 1988	3	Radovčić, 1988	Y	Y	Y	Y	3.6730	Prd
KRP D111	L	Krapina, Croatia	*Homo neanderthalensis*	Radovčić, 1988	3	Radovčić, 1988	Y	Y	Y	Y	3.7584	—
KRP D114	L	Krapina, Croatia	*Homo neanderthalensis*	Radovčić, 1988	2	Radovčić, 1988	Y	Y	Y	Y	3.6670	—
SCLA 4A 6	R	Scladina, Belgium	*Homo neanderthalensis*	Toussaint et al., 1998	2	Toussaint et al., 1998	Y	Y	Y	Y	3.5907	—
Qafzeh 10	R	Qafzeh, Israel	Fossil *Homo sapiens*	Vandermeersch, 1981	1	Vandermeersch, 1981	Y	Y	Y	Y	3.5243	—
Qafzeh 11	R	Qafzeh, Israel	Fossil *Homo sapiens*	Vandermeersch, 1981	1	Vandermeersch, 1981	Y	Y	Y	Y	3.5129	—
ULAC 1	R	Anatomical collection	*Homo sapiens*	ULAC records	1	ULAC records	Y	Y	Y	Y	3.4743	—
ULAC 58	L	Anatomical collection	*Homo sapiens*	ULAC records	1	ULAC records	Y	Y	Y	Y	3.4947	—
ULAC 66	L	Anatomical collection	*Homo sapiens*	ULAC records	1	ULAC records	Y	Y	Y	Y	3.3777	Prd
ULAC 74	L	Anatomical collection	*Homo sapiens*	ULAC records	1	ULAC records	N	Y	Y	N	-	—
ULAC 171	L	Anatomical collection	*Homo sapiens*	ULAC records	1	ULAC records	N	Y	Y	N	-	—
ULAC 522	L	Anatomical collection	*Homo sapiens*	ULAC records	1	ULAC records	N	Y	Y	N	-	—

ULAC 536	R	Anatomical collection	*Homo sapiens*	ULAC records	1	ULAC records	Y	Y	Y	Y	3.3654	Prd
ULAC 607	R	Anatomical collection	*Homo sapiens*	ULAC records	1	ULAC records	N	Y	Y	N	-	—
ULAC 790	L	Anatomical collection	*Homo sapiens*	ULAC records	1	ULAC records	Y	Y	Y	Y	3.4378	—
ULAC 797	R	Anatomical collection	*Homo sapiens*	ULAC records	1	ULAC records	Y	Y	Y	Y	3.5050	—
ULAC 801	L	Anatomical collection	*Homo sapiens*	ULAC records	1	ULAC records	Y	Y	Y	Y	3.5683	—
ULAC 806	L	Anatomical collection	*Homo sapiens*	ULAC records	1	ULAC records	Y	Y	Y	Y	3.5033	—

Abbreviations: EDJ+CEJ = analysis using all landmark sets; EDJ only = analysis using only enamel-dentine junction (EDJ) ridge and EDJ main landmark sets; CEJ only = analysis using only cementum-enamel junction (CEJ) ridge landmark set; CEJ+Med = analysis using CEJ ridge set and single metaconid (Med) landmark; ln(CS) = natural logarithm of centroid size (listed for those specimens included in the EDJ+CEJ analysis); Recon? = specimens with reconstructed dentine horns (Prd = protoconid reconstructed; Med = metaconid reconstructed).

[a] Position basis; 1 = In jaw, 2 = Associated dentition, 3 = Based on morphology.

SOM Table S2

Additional information on the modern human sample, as listed in the records of the Anatomical Collection of the University of Leipzig

Specimen number	Region	Age	Sex
ULAC_1	Germany/Rheinland	Adult	Male
ULAC_58	Norway	Adult	Male
ULAC_66	Norway/Sweden	Adult	Female
ULAC_74	Italy (Etruscan, Tarquinii)	Adult	Male
ULAC_171	Italy (Etruscan, Tarquinii)	Adult	Male
ULAC_522	Egypt (Thebes)	Adult	Male
ULAC_536	Egypt (Thebes)	Adult	Male
ULAC_607	Egypt (Thebes)	Adult	Male
ULAC_790	Africa (Americans/New Orleans)	Adult	Male
ULAC_797	Africa (Americans/New Orleans)	Adult	Male
ULAC_801	Africa (Americans/New Orleans)	Adult	Female
ULAC_806	Africa (Americans/New Orleans)	Adult	Male

SOM Table S3

Canonical variates analysis (CVA) classifications by taxon. The number of principal components used each analysis is indicated in brackets

Specimen	Correct taxon	EDJ+CEJ (7)	EDJ only (5)	CEJ only (4)	CEJ+Med (5)
ZMB 85368	*Hylobates*	*Hylobates*	*Hylobates*	*Hylobates*	*Hylobates*
ZMB 7814	*Hylobates*	*Hylobates*	*Hylobates*	*Hylobates*	*Hylobates*
ZMB 7826	*Hylobates*	*Hylobates*	*Hylobates*	*Hylobates*	*Hylobates*
ZMB 7828	*Hylobates*	*Hylobates*	*Hylobates*	*Hylobates*	*Hylobates*
ZMB 6957	*Pongo*	*Pongo*	*Pongo*	*Pongo*	*Pongo*
ZMB 12209	*Pongo*	*Pongo*	*Pongo*	*Pongo*	*Pongo*
ZMB 38607	*Pongo*	*Pongo*	*Pongo*	*Pongo*	*Pongo*
ZMB 6948	*Pongo*	*Pongo*	*Pongo*	*Pongo*	*Pongo*
ZMB 83509	*Pongo*	*Pongo*	*Pongo*	*Pongo*	*Pongo*
ZMB 83511	*Pongo*	*Pongo*	*Pongo*	*Gorilla*	*Pongo*
ZMB 17963	*Gorilla*	*Gorilla*	*Gorilla*	*Gorilla*	*Gorilla*
ZMB 30941	*Gorilla*	*Gorilla*	*Gorilla*	*Gorilla*	*Gorilla*
ZMB 31435	*Gorilla*	*Gorilla*	*Gorilla*	*Pongo*	*Gorilla*
ZMB 83561	*Gorilla*	*Gorilla*	*Gorilla*	*Gorilla*	*Gorilla*
ZMB 30940	*Gorilla*	*Gorilla*	*Gorilla*	*Pongo*	*Gorilla*
ZMB 11776	*Pan*	*Pan*	*Pan*	*Pan*	*Pan*
ZMB 11800	*Pan*	*Pan*	*Pan*	*Pan*	*Pan*
ZMB 11903	*Pan*	*Pan*	*Pan*	*Pan*	*Pan*
ZMB 13430	*Pan*	*Pan*	*Pan*	*Pan*	*Pan*
ZMB 13437	*Pan*	*Pan*	*Pan*	*Pan*	*Pan*
KNM-KP 29281	*A. anamensis*	*A. anamensis*	*A. anamensis*	*A. anamensis*	*A. anamensis*

KNM-KP 29286	*A. anamensis*	*A. anamensis*	*A. anamensis*	*A. anamensis*	*A. anamensis*
KNM-KP 53160	*A. anamensis*	*A. afarensis*	*A. anamensis*	*A. afarensis*	*A. afarensis*
AL277-1	*A. afarensis*	—	—	*P. robustus*	—
AL333w-1c	*A. afarensis*	*A. africanus*	*A. africanus*	*A. africanus*	*A. africanus*
AL1045	*A. afarensis*	—	—	*A. anamensis*	—
AL128-23	*A. afarensis*	—	—	*H. neanderthalensis*	*A. afarensis*
AL266-1	*A. afarensis*	*A. afarensis*	*A. afarensis*	*A. africanus*	*A. africanus*
AL333-10	*A. afarensis*	*A. africanus*	*A. africanus*	*A. africanus*	*A. africanus*
AL400-1a	*A. afarensis*	—	—	*A. africanus*	—
AL417-1a	*A. afarensis*	—	—	*H. neanderthalensis*	*H. neanderthalensis*
AL655-1	*A. afarensis*	*A. africanus*	*A. afarensis*	*A. africanus*	*A. africanus*
STS24	*A. africanus*	—	*A. afarensis*	—	—
STS51	*A. africanus*	*A. afarensis*	*A. africanus*	*A. africanus*	*A. africanus*
STS52b	*A. africanus*	*A. afarensis*	*A. africanus*	*A. africanus*	*A. africanus*
STW104	*A. africanus*	—	*P. robustus*	—	—
STW142	*A. africanus*	—	—	*P. robustus*	*A. afarensis*
STW193	*A. africanus*	—	—	*A. africanus*	—
STW213	*A. africanus*	*A. afarensis*	*A. afarensis*	*H. naledi*	*A. afarensis*
STW401	*A. africanus*	—	—	*P. robustus*	*P. robustus*
STW404	*A. africanus*	*A. africanus*	*A. africanus*	*P. robustus*	*A. afarensis*
STW498c	*A. africanus*	—	—	*P. robustus*	*A. africanus*
STW420B	*A. africanus*	—	*A. africanus*	—	—
STW7	*A. africanus*	*A. africanus*	*A. africanus*	*A. africanus*	*A. africanus*
Taung1	*A. africanus*	—	*A. afarensis*	—	—
DNH 107	*P. robustus*	—	*P. robustus*	—	—

DNH 46	*P. robustus*	*P. robustus*	*P. robustus*	*A. africanus*	*A. africanus*
DNH 51	*P. robustus*	—	—	*P. robustus*	—
DNH 8	*P. robustus*	*P. robustus*	*P. robustus*	*A. africanus*	*P. robustus*
SK100	*P. robustus*	*P. robustus*	*P. robustus*	*P. robustus*	*P. robustus*
SK23	*P. robustus*	—	—	*P. robustus*	*P. robustus*
SK30	*P. robustus*	—	—	*A. afarensis*	—
SK61	*P. robustus*	—	*P. robustus*	—	—
SK62	*P. robustus*	—	*P. robustus*	—	—
SK63	*P. robustus*	—	*P. robustus*	—	—
SK857	*P. robustus*	*P. robustus*	*P. robustus*	*P. robustus*	*P. robustus*
SKW5	*P. robustus*	*P. robustus*	*H. naledi*	*A. afarensis*	*A. africanus*
UW101-001	*H. naledi*	—	—	*A. anamensis*	*H. naledi*
UW101-1283	*H. naledi*	*H. naledi*	*H. naledi*	*H. naledi*	*H. naledi*
UW101-144	*H. naledi*	*H. naledi*	*H. naledi*	*H. naledi*	*H. naledi*
UW101-1565	*H. naledi*	*H. naledi*	*H. naledi*	*H. naledi*	*H. naledi*
UW101-850	*H. naledi*	—	—	*H. naledi*	—
UW101-889	*H. naledi*	*H. naledi*	*H. naledi*	*H. naledi*	*H. naledi*
UW102-23	*H. naledi*	—	—	*A. afarensis*	—
Combe-Grenal I	*H. neanderthalensis*	*H. neanderthalensis*	*H. neanderthalensis*	*H. neanderthalensis*	*H. neanderthalensis*
Combe-Grenal XV	*H. neanderthalensis*	—	—	*H. sapiens*	*H. sapiens*
KRP 58	*H. neanderthalensis*	—	—	*H. neanderthalensis*	*H. neanderthalensis*
KRP 51	*H. neanderthalensis*	*H. neanderthalensis*	*H. neanderthalensis*	*H. neanderthalensis*	*H. neanderthalensis*
KRP 52	*H. neanderthalensis*	*H. neanderthalensis*	*H. neanderthalensis*	*H. neanderthalensis*	*H. neanderthalensis*
KRP 54	*H. neanderthalensis*	*H. neanderthalensis*	*H. neanderthalensis*	*H. neanderthalensis*	*H. neanderthalensis*
KRP 55	*H. neanderthalensis*	*H. neanderthalensis*	*H. neanderthalensis*	*H. neanderthalensis*	*H. neanderthalensis*

KRP D111	*H. neanderthalensis*	*H. neanderthalensis*	*H. neanderthalensis*	*H. neanderthalensis*	*H. neanderthalensis*
KRP D114	*H. neanderthalensis*	*H. neanderthalensis*	*H. neanderthalensis*	*H. neanderthalensis*	*H. neanderthalensis*
KRP D27	*H. neanderthalensis*	—	—	*H. neanderthalensis*	*H. neanderthalensis*
KRP D28	*H. neanderthalensis*	—	—	*H. neanderthalensis*	*H. neanderthalensis*
KRP D29	*H. neanderthalensis*	—	—	*H. neanderthalensis*	*H. neanderthalensis*
KRP D33	*H. neanderthalensis*	*H. neanderthalensis*	*H. neanderthalensis*	*H. neanderthalensis*	*H. neanderthalensis*
KRP D34	*H. neanderthalensis*	*H. neanderthalensis*	*H. neanderthalensis*	*H. neanderthalensis*	*H. neanderthalensis*
SCLA 4A 6	*H. neanderthalensis*	*H. neanderthalensis*	*H. neanderthalensis*	*H. neanderthalensis*	*H. neanderthalensis*
ULAC 171	*H. sapiens*	—	—	*H. sapiens*	*H. sapiens*
ULAC 1	*H. sapiens*	*H. sapiens*	*H. sapiens*	*H. sapiens*	*H. sapiens*
ULAC 522	*H. sapiens*	—	—	*H. sapiens*	*H. sapiens*
ULAC 536	*H. sapiens*	*H. sapiens*	*H. sapiens*	*H. sapiens*	*H. sapiens*
ULAC 58	*H. sapiens*	*H. sapiens*	*H. neanderthalensis*	*H. sapiens*	*H. sapiens*
ULAC 607	*H. sapiens*	—	—	*H. sapiens*	*H. sapiens*
ULAC 66	*H. sapiens*	*H. sapiens*	*H. sapiens*	*H. sapiens*	*H. neanderthalensis*
ULAC 74	*H. sapiens*	—	—	*H. sapiens*	*H. sapiens*
ULAC 790	*H. sapiens*	*H. sapiens*	*H. sapiens*	*H. sapiens*	*H. sapiens*
ULAC 797	*H. sapiens*	*H. sapiens*	*H. sapiens*	*H. sapiens*	*H. sapiens*
ULAC 801	*H. sapiens*	*H. sapiens*	*A. africanus*	*H. naledi*	*H. neanderthalensis*
ULAC 806	*H. sapiens*	*H. sapiens*	*H. sapiens*	*H. sapiens*	*H. sapiens*
Classification accuracy:		88%	87%	69%	80%

Abbreviations: EDJ+CEJ = analysis using all landmark sets; EDJ only = analysis using only enamel-dentine junction (EDJ) ridge and EDJ main landmark sets; CEJ only = analysis using only cementum-enamel junction (CEJ) ridge landmark set; CEJ+Med = analysis using CEJ ridge set and single metaconid (Med) landmark. See main text for details.

SOM References

Berger, L.R., Hawks, J., de Ruiter, D.J., Churchill, S.E., Schmid, P., Delezene, L.K., Kivell, T.L., Garvin, H.M., Williams, S.A., DeSilva, J.M., Skinner, M.M., Musiba, C.M., Cameron, N., Holliday, T.W., Harcourt-Smith, W., Ackermann, R.R., Bastir, M., Bogin, B., Bolter, D., Brophy, J., Cofran, Z.D., Congdon, K.A., Deane, A.S., Dembo, M., Drapeau, M., Elliott, M.C., Feuerriegel, E.M., Garcia-Martinez, D., Green, D.J., Gurtov, A., Irish, J.D., Kruger, A., Laird, M.F., Marchi, D., Meyer, M.R., Nalla, S., Negash, E.W., Orr, C.M., Radovcic, D., Schroeder, L., Scott, J.E., Throckmorton, Z., Tocheri, M.W., VanSickle, C., Walker, C.S., Wei, P., Zipfel, B., 2015. *Homo naledi*, a new species of the genus *Homo* from the Dinaledi Chamber, South Africa. eLife 4, e09560.

Brain, C.K., 1981. The Hunters or the Hunted? An Introduction to African Cave Taphonomy. University of Chicago Press, Chicago.

Broom, R., Robinson, J.T., 1952. Swartkrans Ape-Man: *Paranthropus crassidens*. Transvaal Museum, Pretoria.

Brown, B., Brown, F.H., Walker, A., 2001. New hominids from the Lake Turkana basin, Kenya. Journal of Human Evolution 41, 29-44.

Dart, R.A., 1925. *Australopithecus africanus* the man-ape of South Africa. Nature 115, 195–199.

Dart, R.A., 1954. The second, or adult, female mandible of *Australopithecus prometheus*. American Journal of Physical Anthropology 12, 313-344.

Garralda, M.-D., Vandermeersch, B., 2000. Les Néandertaliens de la grotte de Combe-Grenal (Domme, Dordogne, France)/The Neanderthals from Combe-Grenal cave (Domme, Dordogne, France). Paléo 12, 213-259.

Grine, F.E., 1989. New hominid fossils from the Swartkrans Formation (1979–1986 excavations): craniodental specimens. American Journal of Physical Anthropology 79, 409-449.

Grine, F.E., Daegling, D.J., 1993. New mandible of *Paranthropus robustus* from Member 1, Swartkrans Formation, South Africa. Journal of Human Evolution 24, 319-333.

Hawks, J., Elliott, M., Schmid, P., Churchill, S.E., Ruiter, D.J.d., Roberts, E.M., Hilbert-Wolf, H., Garvin, H.M., Williams, S.A., Delezene, L.K., Feuerriegel, E.M., Randolph-Quinney, P., Kivell, T.L., Laird, M.F., Tawane, G., DeSilva, J.M., Bailey, S.E., Brophy, J.K., Meyer, M.R., Skinner, M.M., Tocheri, M.W., VanSickle, C., Walker, C.S., Campbell, T.L., Kuhn, B., Kruger, A., Tucker, S., Gurtov, A., Hlophe, N., Hunter, R., Morris, H., Peixotto, B., Ramalepa, M., Rooyen, D.v., Tsikoane, M., Boshoff, P., Dirks, P.H.G.M., Berger, L.R., 2017. New fossil remains of *Homo naledi* from the Lesedi Chamber, South Africa. eLife 6, e24232.

Johanson, D.C., White, T.D., Coppens, Y., 1982. Dental remains from the Hadar Formation, Ethiopia: 1974–1977 collections. American Journal of Physical Anthropology 57, 545-603.

Kimbel, W.H., Delezene, L.K., 2009. “Lucy” redux: A review of research on *Australopithecus afarensis*. American Journal of Physical Anthropology 140, 2-48.

Kimbel, W.H., Johanson, D.C., Rak, Y., 1994. The first skull and other new discoveries of *Australopithecus afarensis* at Hadar, Ethiopia. Nature 368, 449.

Leakey, M.G., Feibel, C.S., McDougall, I., Walker, A., 1995. New four-million-year-old hominid species from Kanapoi and Allia Bay, Kenya. Nature 376, 565.

Leakey, R., Walker, A., 1988. New *Australopithecus boisei* specimens from east and west Lake Turkana, Kenya. American Journal of Physical Anthropology 76, 1-24.

Leakey, R., Wood, B., 1974. New evidence of the genus *Homo* from East Rudolf, Kenya (IV). American Journal of Physical Anthropology 41, 237-243.

Moggi-Cecchi, J., Grine, F.E., Tobias, P.V., 2006. Early hominid dental remains from Members 4 and 5 of the Sterkfontein Formation (1966–1996 excavations): Catalogue, individual associations, morphological descriptions and initial metrical analysis. Journal of Human Evolution 50, 239-328.

Moggi-Cecchi, J., Tobias, P.V., Beynon, A., 1998. The mixed dentition and associated skull fragments of a juvenile fossil hominid from Sterkfontein, South Africa. American Journal of Physical Anthropology 106, 425-465.

Moggi-Cecchi, J., Menter, C., Boccone, S., Keyser, A., 2010. Early hominin dental remains from the Plio-Pleistocene site of Drimolen, South Africa. Journal of Human Evolution 58, 374-405.

Oakley, K.P., Campbell, B.G., Molleson, T.I., Museum, B., 1977. Catalogue of Fossil Hominids. Part I: Africa. Trustees of the British Museum (Natural History), London.

Prat, S., Brugal, J.-P., Roche, H., Texier, P.-J., 2003. Nouvelles découvertes de dents d'hominidés dans le membre Kaitio de la formation de Nachukui (1, 65–1, 9 Ma), Ouest du lac Turkana (Kenya). Comptes Rendus Palevol 2, 685-693.

Radovčić, J., 1988. The Krapina Hominids: An Illustrated Catalog of Skeletal Collection. Mladost, Zagreb.

Robinson, J.T., 1956. The Dentition of Australopithecinae. Transvaal Museum, Pretoria.

Schoetensack, O., 1908. Der Unterkiefer des *Homo heidelbergensis* aus den Sanden von Mauer bei Heidelberg. Ein Beitrag zur Paläontologie des Menschen. Zeitschrift für Induktive Abstammungs-und Vererbungslehre 1, 408-410.

Suwa, G., 1990. A Comparative analysis of hominid dental remains from the Sungura and Usno Formations. Omo Valley, Ethiopia. Ph.D. Dissertation, University of California, Berkeley.

Suwa, G., White, T.D., Howell, F.C., 1996. Mandibular postcanine dentition from the Shungura Formation, Ethiopia: Crown morphology, taxonomic allocations, and Plio-Pleistocene hominid evolution. American Journal of Physical Anthropology 101, 247-282.

Tobias, P.V., 1971. Human skeletal remains from the Cave of Hearths, Makapansgat, northern Transvaal. American Journal of Physical Anthropology 34, 335-367.

Toussaint, M., Otte, M., Bonjean, D., Bocherens, H., Falguères, C., Yokoyama, Y., 1998. Les restes humains néandertaliens immatures de la couche 4A de la grotte Scladina (Andenne, Belgique). Comptes Rendus de l'Académie des Sciences Paris 326, 737-742.

Vandermeersch, B., 1981. Les Hommes Fossiles de Qafzeh (Israël). Editions du Centre National de la Recherche Scientifique, Paris.

Walker, A., Leakey, R.E. (Eds.), 1993. The Nariokotome *Homo erectus* Skeleton. Harvard University Press, Cambridge

Ward, C.V., Leakey, M.G., Walker, A., 2001. Morphology of *Australopithecus anamensis* from Kanapoi and Allia Bay, Kenya. Journal of Human Evolution 41, 255-368.

Ward, C.V., Plavcan, J.M., Manthi, F.K., 2017. New fossils of *Australopithecus anamensis* from Kanapoi, West Turkana, Kenya (2012–2015). Journal of Human Evolution. https://doi.org/10.1016/j.jhevol.2017.07.008

Wood, B., 1991. Koobi Fora Research Project Volume 4: Hominid Cranial Remains from Koobi Fora. Clarendon, Oxford.

Wood, B., Leakey, M., 2011. The Omo-Turkana Basin fossil hominins and their contribution to our understanding of human evolution in Africa. Evolutionary Anthropology 20, 264-292.